

1 **Heterogeneous Interactions between SO<sub>2</sub> and**  
2 **Organic Peroxides in Submicron Aerosol**

3  
4 Shunyao Wang<sup>1</sup>, Tengyu Liu<sup>2</sup>, Jinmyung Jang<sup>1</sup>,  
5 Jonathan P.D. Abbatt<sup>2</sup> and Arthur W.H. Chan<sup>1\*</sup>  
6  
7  
8  
9

10 <sup>1</sup>Department of Chemical Engineering and Applied Chemistry, University of Toronto,  
11 Toronto, Ontario, M5S 3E5, Canada

12 <sup>2</sup>Department of Chemistry, University of Toronto, Toronto, Ontario, M5S 3H6, Canada  
13  
14  
15  
16  
17  
18  
19  
20

21 *\*Correspondence to:* Arthur W.H. Chan (arthurwh.chan@utoronto.ca)

## 22 **Abstract**

23 Atmospheric models often underestimate particulate sulfate, a major component in ambient  
24 aerosol, suggesting missing sulfate formation mechanisms. Heterogeneous reactions between  
25 SO<sub>2</sub> and aerosol play an important role in particulate sulfate formation and its physicochemical  
26 evolution. Here we study the reactive uptake kinetics of SO<sub>2</sub> onto aerosol containing organic  
27 peroxides. We present chamber studies of SO<sub>2</sub> reactive uptake performed under different relative  
28 humidities (RH), particulate peroxide contents, peroxide types, and aerosol acidities. Using  
29 different model organic peroxides mixed with ammonium sulfate particles, SO<sub>2</sub> uptake  
30 coefficient ( $\gamma_{\text{SO}_2}$ ) was found to be exponentially dependent on RH.  $\gamma_{\text{SO}_2}$  increases from 10<sup>-3</sup> at RH  
31 25% to 10<sup>-2</sup> at RH 71% as measured for an organic peroxide with multiple O-O groups. Under  
32 similar conditions, the kinetics in this study were found to be structurally dependent: organic  
33 peroxides with multiple peroxide groups have a higher  $\gamma_{\text{SO}_2}$  than those with only one peroxide  
34 group, consistent with the reactivity trend observed previously in the aqueous phase. In addition,  
35  $\gamma_{\text{SO}_2}$  is linearly related to particle-phase peroxide content, which in turn depends on gas-particle  
36 partitioning of organic peroxides. Aerosol acidity plays a complex role in determining SO<sub>2</sub>  
37 uptake rate, influenced by the effective Henry's Law constant of SO<sub>2</sub> and the condensed phase  
38 kinetics of the peroxide-SO<sub>2</sub> reaction in the highly concentrated aerosol phase. These uptake  
39 coefficients are consistently higher than those calculated from the reaction kinetics in the bulk  
40 aqueous phase, and we show experimental evidence suggesting that other factors, such as  
41 particle-phase ionic strength, can play an essential role in determining the uptake kinetics.  $\gamma_{\text{SO}_2}$   
42 for different types of secondary organic aerosol (SOA) were measured to be on the order of 10<sup>-4</sup>.  
43 Overall, this study provides quantitative evidence of the multiphase reactions between SO<sub>2</sub> and  
44 organic peroxides, highlighting the important factors that govern the uptake kinetics.

## 45 **Introduction**

46 Sulfate and organic compounds are ubiquitous particulate components in both polluted and  
47 pristine environments (Chen et al., 2009;Andreae et al., 2018;He et al., 2011;Sun et al.,  
48 2013;Huang et al., 2014), with important implications for public health and global climate  
49 (Hallquist et al., 2009). Particulate sulfate can form via S(IV) oxidation by OH radicals in the gas  
50 phase and via oxidation in cloud water, fog droplets or the aerosol aqueous phase, including by  
51 H<sub>2</sub>O<sub>2</sub>, O<sub>2</sub> (catalyzed by transition metals), O<sub>3</sub>, NO<sub>2</sub> and small organic peroxides (methyl  
52 hydroperoxide and peroxyacetic acid) (Seinfeld and Pandis, 2012). However, atmospheric  
53 models tend to underestimate particulate sulfate production on both global (Tie et al., 2001;Yang  
54 et al., 2017;Fairlie et al., 2010) and regional scales, especially during heavy haze episodes (Wang  
55 et al., 2014;Zheng et al., 2015;Sha et al., 2019;Gao et al., 2016;Li et al., 2017;Huang et al.,  
56 2019), suggesting that the overall kinetics may be underestimated and/or important mechanisms  
57 may be missing in models.

58 To reconcile these differences, studies have investigated novel reaction mechanisms of sulfate  
59 formation. Stabilized Criegee intermediates (sCIs) were hypothesized to oxidize SO<sub>2</sub> rapidly and  
60 potentially serve as an important source of ambient sulfate (Mauldin et al., 2012). In the work by  
61 Newland et al. (2015) and Nguyen et al. (2016), this sCIs pathway was shown to play a minor  
62 role in sulfate formation. More recently, when Liu et al. (2019) applied this mechanism and  
63 kinetics to a source-oriented WRF-Chem model, the sCIs pathway was found to only account for  
64 at most 9% of the total particulate sulfate. Reactive nitrogen species (such as NO<sub>2</sub>) have also  
65 been put forward to account for the missing sulfate at relatively high aerosol pH (close to 7)  
66 (Wang et al., 2016;Cheng et al., 2016). However, such high aerosol pH is not substantiated by  
67 thermodynamic models, which conclude that pH ranges between 4 and 5 even in polluted regions

68 (Song et al., 2018;Guo et al., 2017). A recent modeling study incorporating this heterogeneous  
69  $\text{NO}_x$  mechanism still exhibited a discrepancy of 20% between the predicted and observed sulfate,  
70 indicating the possibility of unknown mechanisms (Huang et al., 2019). Other factors may play a  
71 role in enhancing the particle-phase sulfate formation rates. Chen et al. (2019) investigated the  
72 synergistic effects of  $\text{NO}_2$  and  $\text{NH}_3$  on sulfate formation, and found that the rate of this reaction  
73 can be enhanced by the high ionic strength in the particle phase. This enhancement effect by  
74 solute strength on sulfate formation was also investigated for the  $\text{H}_2\text{O}_2$  pathway in aerosol liquid  
75 water. Liu et al. (2020) found ionic strength and general acid-catalyzed mechanisms can cause  
76 the S(VI) formation rate to be nearly 50 times faster in aerosol phase than in dilute solutions. On  
77 the other hand, during the severe haze episodes in China (Li et al., 2020; Guo et al., 2017),  
78 transition metal ion (TMI) catalysis of  $\text{SO}_2$  oxidation by  $\text{O}_2$  can be significantly suppressed in the  
79 aerosol phase due to high ionic strength (Liu et al., 2020;Cheng et al., 2016; Su et al., 2020).  
80 In addition to high solute strength, submicron aerosol is also rich in organic compounds (Jimenez  
81 et al., 2009;Hallquist et al., 2009). In recent years, many studies have investigated the potential  
82 role of heterogeneous interactions between  $\text{SO}_2$  and organic aerosol on particulate sulfate  
83 formation. Song et al. (2019) found heterogeneous oxidation of hydroxymethanesulfonate  
84 (HMS) by OH can trigger rapid sulfate formation. Wang et al. (2020) studied photosensitizers in  
85 ambient particles and found this pathway could be essential under specific light conditions.  
86 Recent studies found reactive intermediates from isoprene oxidation (Huang et al., 2019) and  
87 benzoic acid (Huang et al., 2020), can yield a variety of organosulfur species upon catalysis by  
88 TMI. Other studies have also investigated the interactions between secondary organic aerosol  
89 (SOA) and  $\text{SO}_2$ . Field observations found that ambient sulfate abundance is highly correlated  
90 with SOA formation (Yee et al., 2020;Xu et al., 2015). Liu et al. (2019) found that  $\text{SO}_2$  enhances

91 SOA formation and average carbon oxidation state during methoxyphenol photooxidation. By  
92 performing chamber experiments with limonene SOA formation in the presence of SO<sub>2</sub>, Ye et al.  
93 (2018) also observed significant SO<sub>2</sub> decay along with increased SOA yields and carbon  
94 oxidation state, proposing that organic peroxides in SOA may be the key reactive intermediates  
95 for SO<sub>2</sub> oxidation.

96 Organic peroxides are key intermediates for aerosol formation and ubiquitously exist in many  
97 SOA systems (Hallquist et al., 2009; Bianchi et al., 2019). Numerous studies have reported  
98 peroxide content of 20-60% for isoprene and monoterpene derived SOA (Surratt et al., 2006; Ng  
99 et al., 2008; Ye et al., 2018; Epstein et al., 2014). A significant fraction of organic peroxide (30%-  
100 50%) has also been found in naphthalene-derived SOA under low/high NO<sub>x</sub> conditions  
101 (Kautzman et al., 2009). Using model simulations, Bonn et al. (2004) found organic  
102 hydroperoxides can account for up to 60% of global SOA. The aqueous phase reaction kinetics  
103 between organic peroxides and dissolved SO<sub>2</sub> have been explored in previous studies (Lind et al.,  
104 1987; Gunz and Hoffmann, 1990; Wang et al., 2019; Dovrou et al., 2019; Yao et al., 2019). The  
105 second order reaction rate constants for organic peroxides in SOA (Dovrou et al., 2019; Yao et  
106 al., 2019) and S(IV) were measured to be on the order of 10<sup>2</sup>-10<sup>3</sup> M<sup>-1</sup> s<sup>-1</sup>, which are within the  
107 range of those measured for commercially available organic peroxides (Wang et al., 2019) and  
108 small organic peroxides (Lind et al., 1987). Yao et al. (2019) quantified the reactive uptake  
109 coefficient of SO<sub>2</sub> ( $\gamma_{\text{SO}_2}$ ) onto  $\alpha$ -pinene SOA to be on the order of 10<sup>-4</sup>-10<sup>-3</sup>, which is positively  
110 dependent on RH and inferred particle-phase peroxide content. These reactions are also linked to  
111 the formation of organosulfates (Wang et al., 2019). Both inorganic sulfate (85-90%) and  
112 organosulfates (10-15%) were observed as products of SO<sub>2</sub> reactive uptake onto SOA (Yao et al.,  
113 2019).

114 Given the potential significance of SO<sub>2</sub> reactive uptake in particulate sulfate formation, a more  
115 in-depth study is needed to determine the important factors that govern the heterogeneous  
116 kinetics of SO<sub>2</sub> onto organic peroxide containing aerosol. In this study, we measured  $\gamma_{\text{SO}_2}$  for two  
117 categories of aerosol: 1. Model organic peroxides mixed with ammonium sulfate or malonic acid  
118 and 2. SOA from a few representative biogenic and anthropogenic precursors. The impacts of  
119 RH, peroxide type, peroxide content, and condensed phase pH on SO<sub>2</sub> reactive uptake were  
120 evaluated systematically with the goal of better understanding atmospheric multiphase sulfate  
121 formation.

122

## 123 **2. Methods**

124 The reactive uptake of SO<sub>2</sub> onto peroxide-containing particles was studied in a 1 m<sup>3</sup> Teflon  
125 chamber under ambient temperature and pressure. In brief, generated particles and SO<sub>2</sub> were  
126 introduced into the chamber separately. The consumption of SO<sub>2</sub>, changes in particle size  
127 distribution and chemical composition were monitored to estimate the reactive uptake  
128 coefficients. Particles were also collected on filters for offline chemical characterization.

129

### 130 **2.1 Seed aerosol generation**

131 In this work, two types of aerosol were used to investigate the uptake of SO<sub>2</sub>. The first is  
132 ammonium sulfate or malonic acid mixed with model organic peroxides (Fig. S1). In this first set  
133 of experiments, an aerosol atomizer (Model 3076, TSI Inc., USA) was used to generate aqueous  
134 particles from dilute solution. Each solution consists of ammonium sulfate ( $\geq 99\%$ , Sigma-  
135 Aldrich) or malonic acid (99%, Sigma-Aldrich) and a model organic peroxide in ultrapure water  
136 (HPLC grade, Fisher Chemical). For the experiments investigating the relationship between  $\gamma_{\text{SO}_2}$

137 and peroxide type (Expt. 2-14, Table S1), different commercially available organic peroxides  
138 were used, including tert-butyl hydroperoxide (70 wt. % in water, Sigma-Aldrich), cumene  
139 hydroperoxide (80 wt. % in water, Sigma-Aldrich), and 2-butanone peroxide (40% wt. % in  
140 water, Sigma-Aldrich). The molar ratio of organic peroxide to ammonium sulfate in the  
141 atomizing solution was 2:1 with the aim of being atmospherically relevant (corresponding to  
142 maximum particulate peroxide molar fraction of 66% and mass fraction of approximately 50-  
143 70% if all the organic peroxides were assumed to remain in the particle phase). This ratio was  
144 used as a proxy for total peroxide content in both gas and particle phase relative to that of  
145 ammonium sulfate upon atomization. For the experiments studying the relationship between  $\gamma_{\text{SO}_2}$   
146 and particle-phase peroxide content, the molar ratio of organic peroxide to ammonium sulfate  
147 (Expt. 10-12, 15-18, Table S1) in the solution was adjusted to be 0.02, 0.2, 1, 2, and 4,  
148 respectively. In experiments where malonic acid was used (Expt. 19-22, Table S1), molar ratios  
149 of 0.2, 1, 2, and 4 were adopted. For measuring  $\gamma_{\text{SO}_2}$  with different aerosol pH (Expt. 17, 23-25,  
150 Table S1), different amounts of HCl (37%, Sigma-Aldrich) were added into the solution (0,  
151 0.00002 M, 0.0001 M, 0.001 M HCl) prior to atomization. The initial pH of aerosol (2.5, 2.2,  
152 1.6, 1, respectively) were modeled using E-AIM III model (Clegg et al., 1998) based on the  
153 initial molar ratios of inorganic species ( $\text{H}^+$ ,  $\text{NH}_4^+$ ,  $\text{SO}_4^{2-}$ ,  $\text{Cl}^-$ ) in the atomizing solution and  
154 measured RH (around 50%). The atomized particles were flowed into the chamber without  
155 drying, and therefore assumed to remain deliquesced under the range of RH we studied. Expt. 2-  
156 14 (Table S1) also represent those where the relationship between  $\gamma_{\text{SO}_2}$  and RH conditions were  
157 studied.

158 In the second set of experiments, the uptake of  $\text{SO}_2$  onto SOA was investigated (Fig. S2, Expt.  
159 26-28, Table S1). A custom-built 10 L quartz oxidation flow reactor was used to produce SOA

160 (Ye et al., 2016) from different hydrocarbon precursors. In this work, we studied SOA formed  
161 from toluene photooxidation, limonene ozonolysis and  $\alpha$ -pinene ozonolysis, 3 of the most  
162 commonly studied SOA systems (Ng et al., 2007;Hildebrandt et al., 2009; Hartz et al.,  
163 2005;Varutbangkul et al., 2006). Toluene (analytical standard, Sigma Aldrich) was injected  
164 continuously into zero air flow by a syringe (1000 mL, Hamilton) installed on a syringe pump  
165 (KDS Legato100) to achieve an initial concentration of 0.5 ppm. Limonene (Sigma-Aldrich,  
166 97 %) and  $\alpha$ -pinene (Sigma-Aldrich, 98 %) were pre-dissolved in cyclohexane (Sigma-Aldrich,  
167 99.5 %) with a volumetric ratio of 1: 1500 and 1: 500 to ensure that OH formed from limonene  
168 or  $\alpha$ -pinene ozonolysis is scavenged by cyclohexane, estimated based on the rate constants  
169 (Atkinson and Arey, 2003). The initial steady-state concentrations of limonene and  $\alpha$ -pinene  
170 were controlled to be around 2 ppm and 1 ppm entering the flow tube. O<sub>3</sub>, used as the oxidant  
171 (for limonene and  $\alpha$ -pinene) or the OH precursor (for toluene), was generated by passing 0.5 L  
172 min<sup>-1</sup> pure oxygen (99.6 %, Linde, Mississauga, Canada) through an O<sub>3</sub> generator (no.  
173 97006601, UVP, Cambridge, UK). Humidified air was produced by bubbling zero air through a  
174 custom-made humidifier at a flow rate of 1 L min<sup>-1</sup>. The photolysis of O<sub>3</sub> produces O (<sup>1</sup>D),  
175 which reacts with water vapour to produce ·OH with illumination from the 254 nm UV lamps  
176 (UVP, Cambridge, UK) to initiate the photooxidation of toluene. The average residence time  
177 inside the flow tube was controlled to be around 5 minutes. A gas chromatography–flame  
178 ionization detector (GC-FID, model 8610C, SRI Instruments Inc., LV, USA) equipped with a  
179 Tenax® TA trap was used to monitor the concentration of hydrocarbon precursors at the  
180 inlet/outlet of the flow reactor. In all cases, the O<sub>3</sub> concentration was maintained to be at least 10  
181 times higher than that of the hydrocarbon. Temperature and relative humidity were monitored by  
182 an Omega HX94C RH/T transmitter. Particle size distribution and volume concentration were



183 monitored using a custom-built scanning mobility particle sizer (SMPS), which is a combination  
184 of a differential mobility analyzer column (DMA, model 3081, TSI, Shoreview, MN, USA) with  
185 flow controls and a condensation particle counter (CPC, model 3772, TSI, Shoreview, MN,  
186 USA).

187

## 188 **2.2 Quantification of $\gamma_{SO_2}$**

189 Prior to each experiment, the chamber was flushed by purified air overnight with a flow rate of  
190  $25 \text{ L min}^{-1}$  until particle number concentration was less than  $5 \text{ cm}^{-3}$  and  $\text{SO}_2$  was less than 1 ppb.  
191 To adjust RH, the chamber was humidified by passing purified air through a custom-built  
192 humidifier filled with ultra-pure water. For experiments with atomized ammonium sulfate or  
193 malonic acid,  $\text{SO}_2$  was injected into the chamber prior to the introduction of particles. For  
194 experiments studying  $\gamma_{SO_2}$  onto SOA, aerosol generated from the flow tube was injected into the  
195 Teflon chamber continuously after passing through an  $\text{O}_3$  denuder (Ozone Solutions, Iowa, USA)  
196 to achieve specific aerosol concentration inside the chamber prior to  $\text{SO}_2$  addition.  $\text{SO}_2$  mixing  
197 ratio in the chamber during each experiment was continuously monitored using an  $\text{SO}_2$  analyzer  
198 (Model 43i, Thermo Scientific). The initial mixing ratio of  $\text{SO}_2$  in each experiment was  
199 controlled to be around 200 ppb. Aerosol size distribution was monitored by SMPS. The reactive  
200 uptake coefficient of  $\text{SO}_2$  was calculated by integrating the following equation:

$$201 \quad -\frac{d[\text{SO}_2]}{dt} = \frac{1}{4} \gamma_{SO_2} A \bar{c} [\text{SO}_2] \quad (1)$$

202

203 Where  $[\text{SO}_2]$  is the  $\text{SO}_2$  mixing ratio (ppb) monitored by the  $\text{SO}_2$  analyzer; A is the average  
204 surface area concentration ( $\mu\text{m}^2 \text{ cm}^{-3}$ ) derived from the particle size distribution measured by  
205 SMPS;  $\bar{c}$  represents the mean molecular velocity ( $\text{cm s}^{-1}$ ) of  $\text{SO}_2$ .  $d[\text{SO}_2]/dt$  is solved over the  
206 initial  $\text{SO}_2$  decay, such that the peroxide concentration in the aerosol liquid phase is assumed to

207 be constant and pseudo-first order kinetics can be applied (Abbatt et al., 2012; Thornton et al.,  
208 2003). A summary of all the measured  $\gamma_{\text{SO}_2}$  can be found in Table S1. Typical evolution of  
209 monitored species can be seen in Fig.1. Control experiments were performed in order to rule out  
210 other potential factors (e.g.  $\text{SO}_2$  loss in the in-line filter in front of the  $\text{SO}_2$  analyzer, interferences  
211 inside the  $\text{SO}_2$  analyzer, chamber wall losses,  $\text{SO}_2$  uptake onto wet ammonium sulfate, gas-phase  
212 reaction of  $\text{SO}_2$  with peroxide vapour) that may contribute to the  $\text{SO}_2$  decay observed during the  
213  $\gamma_{\text{SO}_2}$  measurement inside the chamber (Fig. S3-S6). Measurement uncertainty and precision of  
214  $\gamma_{\text{SO}_2}$  in this study can be found in Table S1. Also, we observed there was  $\text{SO}_2$  repartitioning from  
215 the humid chamber wall in the presence of organic peroxide under high RH (Fig. S6b, RH 74%).  
216 The observed  $\text{SO}_2$  repartitioning rate was then applied to correct the  $\gamma_{\text{SO}_2}$  measured under high  
217 RH conditions (above 70%, Expt.14), and this correction amounts to a 40% increase in  
218 calculated  $\gamma_{\text{SO}_2}$ .

219

### 220 **2.3 Offline peroxide quantification**

221 Aerosol was collected onto 47 mm PTFE (polytetrafluoroethylene) filters with 0.2  $\mu\text{m}$  pore size  
222 (Whatman®, GE Healthcare) from the chamber by a diaphragm pump (KNF Neuberger Inc., USA)  
223 for offline chemical analysis. The total particulate peroxide content ( $\text{H}_2\text{O}_2$ , ROOH and ROOR) in  
224 these samples prior to  $\text{SO}_2$  uptake was quantified using the iodometric–spectrophotometric assay  
225 (Docherty et al., 2005).  $\text{I}_2$  produced from the reaction between  $\text{I}^-$  and peroxides can further quickly  
226 combine with the excess amount of  $\text{I}^-$  to form  $\text{I}_3^-$ , which has brown color and absorbs UV-vis at  
227 470nm. The SOA extraction was then aliquoted into a 96-well UV plate (Greiner Bio-One,  
228 Kremsmünster, AT) with 160  $\mu\text{L}$  well<sup>-1</sup>. 20  $\mu\text{L}$  of formic acid ( $\geq 95\%$ , Sigma-Aldrich) was added  
229 into each well, following by 20  $\mu\text{L}$  potassium iodide (BioUltra,  $\geq 99.5\%$ , Sigma-Aldrich) solution

230 (dissolved in DI water). The plate was then covered by an adhesive plate sealer (EdgeBio,  
 231 Gaithersburg, USA) immediately in order to avoid reagent evaporation and O<sub>2</sub> oxidation. After  
 232 incubation for an hour in the dark, the UV-vis absorption at 470nm was measured using a UV-vis  
 233 spectrophotometer (Spectramax 190, Molecular Devices Corporation, Sunnyvale, CA) and then  
 234 converted to peroxide concentration using the calibration curve made by tert-butyl hydroperoxide  
 235 (70 wt. % in H<sub>2</sub>O, Sigma-Aldrich) with a series of concentrations (0-10mM). An average  
 236 molecular mass for seed particles (SOA + ammonium sulfate) was assumed based on the chemical  
 237 composition in order to calculate the molar fraction of total peroxides using the following equation:

$$238 \text{ Molar fraction of peroxide} = \frac{N_{peroxide}}{N_{aerosol}} = N_{peroxide} \frac{M_{(NH_4)_2SO_4} f_{(NH_4)_2SO_4} + M_{peroxide} f_{peroxide}}{m_{aerosol}}$$

240 where  $m_{aerosol}$  is the weighed aerosol mass on the filter;  $M_{(NH_4)_2SO_4}$  and  $M_{peroxide}$  are the  
 241 molecular mass of ammonium sulfate and peroxide, respectively;  $f_{(NH_4)_2SO_4}$  and  $f_{peroxide}$  are the  
 242 initial molar fraction of ammonium sulfate and peroxide;  $N_{peroxide}$  and  $N_{aerosol}$  are the  
 243 measured peroxide molar and calculated aerosol molar, respectively. More details about the  
 244 iodometric-spectrophotometric procedures were described in previous work (Wang et al., 2018).  
 245

246

### 247 **3 Results and discussion**

#### 248 **3.1 SO<sub>2</sub> uptake and RH**

249 A positive relationship between  $\gamma_{SO_2}$  and RH (between 25 and 71%) was observed for all types of  
 250 organic peroxides studied (Fig. 2). The positive dependence of the reactive uptake coefficient of  
 251 water-soluble gaseous species on RH has also been observed in other studies (Thornton et al.,  
 252 2003; Griffiths et al., 2009; Zhao et al., 2017; Zhang et al., 2019). Recently, the uptake behavior of

253 SO<sub>2</sub> onto soot, mineral dust and SOA were also shown to positively depend on RH (Zhang et al.,  
254 2019;Zhao et al., 2017;Yao et al., 2019).

255 It is also noteworthy that an exponential dependence of SO<sub>2</sub> reactive uptake coefficient on RH  
256 was observed in our study.  $\gamma_{\text{SO}_2}$  increases with increased relative humidity, which could even be  
257 more significant under high RH regime. This is consistent with previous laboratory studies that  
258 measured the reactive uptake coefficient of SO<sub>2</sub> onto aerosol to be exponentially dependent on  
259 RH (Zhang et al., 2019;Yao et al., 2019). Additionally, multiple field campaigns have observed  
260 significant correlation between particulate sulfate formation and ambient RH (Song et al.,  
261 2019;Sun et al., 2013;Huang et al., 2020). Sun et al. (2013) observed faster sulfate formation rate  
262 under humid conditions, proposing a significant impact of aerosol liquid water on sulfate  
263 production during wintertime in Beijing. Zheng et al. (2015) reported a notably higher SOR  
264 (molar ratio of sulfate to the sum of sulfate and SO<sub>2</sub>) during wet period (RH>50%), indicating  
265 the importance of heterogeneous reactions to the secondary sulfur transformation with abundant  
266 aerosol water content under humid conditions. In a recent study by Song et al. (2019), the rapid  
267 sulfate formation rate observed under high RH conditions was found to be significantly higher  
268 than atmospheric modeling results implemented with homogeneous SO<sub>2</sub> oxidation pathways,  
269 which was later attributed to heterogeneous sulfate formation mechanisms. Multiple mechanisms  
270 can potentially explain this observed  $\gamma_{\text{SO}_2}$ -RH dependence. An enhanced relative humidity would  
271 result in a nonlinear increase of aerosol water content, which can lead to more SO<sub>2</sub> dissolved in  
272 the aerosol aqueous phase (Seinfeld and Pandis, 2012). It should be noted that while the relative  
273 humidity is varied systematically in these experiments, the relationship is more complex since  
274 RH also affects other aerosol properties which can affect the uptake kinetics in turn. For  
275 example, a higher aerosol liquid water content could dilute protons and thus lower the aerosol

276 acidity. In a study by Laskin et al. (2003), an enhanced uptake of SO<sub>2</sub> onto sea-salt particles was  
277 observed with an increased aerosol alkalinity at high pH range.

### 278 279 **3.2 Dependence of SO<sub>2</sub> uptake on peroxide content and type**

280 As expected, the measured uptake rate of SO<sub>2</sub> is dependent on the particulate peroxide content in  
281 the current study. Fig. 3 shows that  $\gamma_{\text{SO}_2}$  is linearly proportional to the amount of particulate  
282 peroxide for aerosol with similar volume-to-surface ratios and containing the same type of  
283 organic peroxides. This positive relationship between  $\gamma_{\text{SO}_2}$  and condensed phase peroxide content  
284 has also been inferred from experiments of SO<sub>2</sub> uptake onto  $\alpha$ -pinene SOA (Yao et al., 2019),  
285 where the peroxide content in  $\alpha$ -pinene SOA was varied indirectly by introducing NO and  
286 adjusting the branching ratio of the peroxide-yielding RO<sub>2</sub>+HO<sub>2</sub>/RO<sub>2</sub> pathway.

287 In addition to the amount of peroxide injected, the particulate fraction of organic peroxide  
288 available for heterogeneous reaction is also influenced by gas-particle partitioning. As indicated  
289 in Fig. 2, the reactive uptake coefficients of different organic peroxides vary amongst each other  
290 by about an order of magnitude in the range of RH studied, despite the same amounts of peroxide  
291 relative to ammonium sulfate initially in the atomizing solution. Based on our previous work  
292 (Wang et al., 2019), the aqueous-phase rate constants for these organic peroxides with dissolved  
293 S(IV) only vary by a factor of 2-3 and therefore cannot fully explain the observed difference in  
294 uptake rates. Since vapour pressure vary considerably among the different peroxides in the  
295 present study, gas-particle partitioning is likely to influence the amount of peroxide in the  
296 particle phase that react with dissolved SO<sub>2</sub>. The relative particulate peroxide content on filters  
297 of the three peroxides collected from chamber experiments under RH 50% without SO<sub>2</sub> uptake  
298 were measured by the offline KI method (Fig. S7). Although the initial ratio of organic peroxide

299 to ammonium sulfate in the atomizing solution was nominally the same, we measured the highest  
300 amount of particulate peroxide with 2-butanone peroxide (16.7%), followed by cumene  
301 hydroperoxide (12.7%) and then tert-butyl hydroperoxide (3.8%) using the offline iodometric  
302 method. This trend in particulate peroxide content is consistent with the vapour pressures  
303 calculated using the SIMPOL group contribution method (Pankow et al., 2008), with 2-butanone  
304 peroxide being the least volatile, and tert-butyl hydroperoxide being the most volatile. Also, the  
305 order of particle-phase peroxide content is consistent with the order of  $\gamma_{\text{SO}_2}$  observed, as shown in  
306 Fig. 2. A simple visualization of these relationships between different peroxide characteristics  
307 (number of peroxide groups, vapour pressure and aqueous-phase rate constants) and measured  
308  $\gamma_{\text{SO}_2}$  (at RH = 50%) is illustrated in Fig. S7, which indicates higher  $\gamma_{\text{SO}_2}$  can be expected for  
309 organic peroxides with multiple O-O groups, lower vapour pressures and higher aqueous phase  
310 reactivities. It should be noted that the order of magnitude difference in experimentally measured  
311  $\gamma_{\text{SO}_2}$  among various organic peroxides (Fig.2) is still not fully explained when both volatility and  
312 reaction kinetics are taken into account (Fig.S7), suggesting that the reactive uptake may be  
313 influenced by other factors. In summary, for our current experiments where we nominally  
314 maintained total injected amount of organic peroxide constant, measured  $\gamma_{\text{SO}_2}$  depends both on  
315 reactivity and gas-particle partitioning of the organic peroxides.

316

### 317 **3.3 SO<sub>2</sub> uptake and aqueous phase kinetics**

318 Since the aqueous phase reaction rate constants between S(IV) and these model organic  
319 peroxides have been measured previously (Wang et al., 2019), we can test our understanding of  
320 the measured  $\gamma_{\text{SO}_2}$  using a simple model. By assuming the amount of SO<sub>2</sub> dissolved in the aerosol

321 is in equilibrium with the gas phase, the overall  $\gamma_{\text{SO}_2}$  can be expressed using the simplified  
 322 resistor model (Hanson et al., 1994):

323

$$324 \quad \frac{1}{\gamma} = \frac{1}{\alpha} + \frac{\bar{c}}{4HRT\sqrt{k^I D_l}} \frac{1}{\left[\coth(q) - \frac{1}{q}\right]} \quad (2)$$

325 where  $\alpha$  is the mass accommodation coefficient,  $\bar{c}$  is the mean molecular speed of  $\text{SO}_2$  ( $\text{cm s}^{-1}$ ),  
 326  $H$  is the effective Henry's law constant that includes both the dissolution of  $\text{SO}_2$  and the  
 327 dissociation of  $\text{H}_2\text{SO}_3$  ( $\text{M atm}^{-1}$ ),  $R$  is the ideal gas constant ( $\text{atm L mol}^{-1} \text{K}^{-1}$ ),  $T$  is the  
 328 temperature (K), and the parameter  $q$  is used to describe the competition between the reaction  
 329 and diffusion of the dissolved gaseous species within a particle, which is further calculated as:

330

$$331 \quad q = r \sqrt{\frac{k^I}{D_l}} \quad (3)$$

331 where  $r$  is the radius (cm) of a given particle,  $D_l$  is the aqueous-phase diffusion coefficient ( $\text{cm}^2$   
 332  $\text{s}^{-1}$ ),  $k^I$  is the first order rate constant ( $\text{s}^{-1}$ ) for the reaction. For experiments in the current study,  
 333 the calculated  $q$  values were consistently found to be far less than 1, which indicates a volume-  
 334 limited reaction regime. Combining with the assumption of a relatively fast mass  
 335 accommodation process compared with the bulk phase reaction, equation (2) can be further  
 336 simplified as to describes reactive uptake in the volume-limited regime:

337

$$338 \quad \gamma = \frac{4HRT[\text{peroxide}]k^{II} V}{\bar{c} S} \quad (4)$$

338 Here, we assume all the peroxides remain in the condensed phase upon atomizing and reaction  
 339 inside the chamber for the upper-bound prediction of  $\gamma_{\text{SO}_2}$ . [peroxide] represents the particle phase  
 340 concentration of total organic peroxide (M) based on the initial ratio between organic peroxide and  
 341 ammonium sulfate in the atomizing solution, and the aerosol water content output by E-AIM III  
 342 (Clegg et al., 1998),  $k^{II}$  is the second order reaction rate constant ( $\text{M}^{-1} \text{s}^{-1}$ ), which we have  
 343 measured in the bulk phase at dilute concentrations previously (Wang et al., 2019),  $V/S$  is the ratio

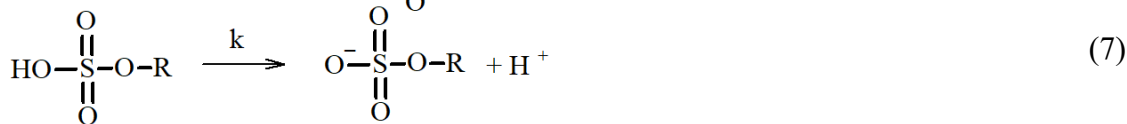
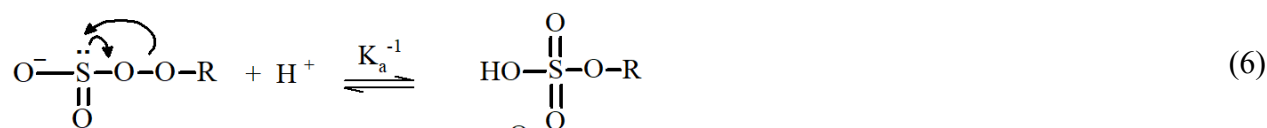
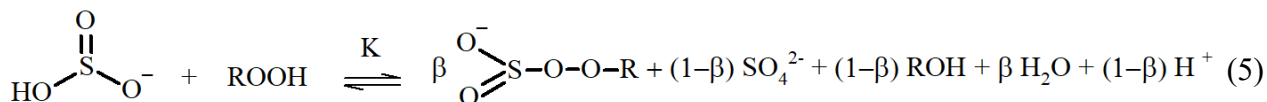
344 between particle volume concentration ( $\mu\text{m}^3 \text{ cm}^{-3}$ ) and particle surface area concentration ( $\mu\text{m}^2$   
345  $\text{cm}^{-3}$ ) derived from SMPS measurements. As a result, the observed reactive uptake coefficient of  
346  $\text{SO}_2$  can be compared to that predicted from the bulk phase reaction rate constant, and the results  
347 are shown in Fig. 4 and Fig. S8. Overall, we noticed that this model captures the dependence of  
348  $\gamma_{\text{SO}_2}$  on peroxide content, but the modeled results were found to be generally 15-50 times lower  
349 than the experimentally measured values (Fig. S8). The current  $\gamma_{\text{SO}_2}$  predictions are likely upper-  
350 bound estimates since all the peroxides were assumed to stay in the condensed phase without  
351 partitioning. As a result, this observed 15-50 times of discrepancy could even be larger if the  
352 particulate peroxide content during the chamber experiments were lower due to partitioning.

353 It should be noted that the calculated  $\gamma_{\text{SO}_2}$  was based on reaction kinetics measured in dilute  
354 solutions while the experimental  $\gamma_{\text{SO}_2}$  were measured directly from suspended particles. This large  
355 difference in kinetics between those in aerosol and in dilute bulk solution suggests that this  
356 multiphase interaction is strongly favored in the highly concentrated aerosol environment. One of  
357 the potential explanations for this discrepancy could be liquid-liquid phase separation (LLPS) in  
358 aerosol between organic peroxide and ammonium sulfate (Ciobanu et al., 2009; O'Brien et al.,  
359 2015) such that  $\text{SO}_2$  can directly interact with the acidic organic phase, where the concentration of  
360 peroxides can be higher and the kinetics can be different from what we have measured in dilute  
361 solution (Wang et al., 2019). However, LLPS is generally governed by the chemical composition  
362 of the hydrophobic phase (Freedman, 2017). A higher level of oxygenation in organic aerosol is  
363 related with higher hydrophilicity, which would favor a homogeneous particle instead of phase  
364 separation. Previous studies showed that LLPS did not occur for organic coating with O:C above  
365 0.8 (You et al., 2013; You et al., 2014). The LLPS phenomenon in simple organic-inorganic  
366 mixtures can also be affected by the functional groups. The maximum O:C for LLPS could be 0.71



367 for organics with multiple carboxylic and hydroxyl groups but low aromatic content (Song et al.,  
 368 2012) while the 2-butanone peroxide we used for both  $\gamma_{\text{SO}_2}$  measurement and prediction in the  
 369 present study has multiple peroxide groups with an O:C value of 0.75. Particle size could also have  
 370 impacts on phase separation (Cheng et al., 2015). Particle diameters in the current study are mainly  
 371 under 200 nm while a previous study showed particles smaller than this size are less likely to  
 372 experience LLPS (Veghte et al., 2013). We therefore believe that LLPS is not likely to be  
 373 responsible for the enhanced uptake rate observed under these experimental conditions.

374 Another explanation is the high solute strength in the concentrated aerosol phase. Although the  
 375 aerosol water content for ammonium sulfate aerosol was found to be higher than that of malonic  
 376 acid aerosol under RH 50%. As indicated in Fig. 4 and Fig. S8, the difference between the  
 377 measured and predicted  $\gamma_{\text{SO}_2}$  is larger for ammonium sulfate aerosol than for malonic acid.  
 378 Meanwhile, the calculated ionic strength in aerosol liquid phase under RH 50% for ammonium  
 379 sulfate ( $40 \text{ mol kg}^{-1}$ ) is significantly larger than that of malonic acid ( $0.45 \text{ mol kg}^{-1}$ ). It has been  
 380 previously reported that the reaction rate between sulfite and hydrogen peroxide in aqueous phase  
 381 increases with ionic strength (Maaß et al., 1999). Based on the reaction mechanisms proposed for  
 382 dissolved  $\text{SO}_2$  and hydrogen peroxide (Halperin and Taube, 1952), we speculate the reaction  
 383 between aqueous phase S(IV) and organic peroxides to follow a similar mechanism:

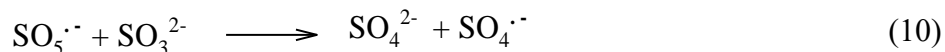
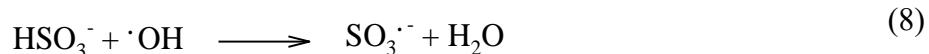


384

385 where the overall rate constant is equal to  $k \frac{K}{K_a}$ , assuming fast equilibrium steps for reactions 5 and  
386 6. Dissociated solutes are surrounded by an extended solvation shell which could affect the  
387 reaction rates (Herrmann, 2003). Fewer available free water molecules would therefore shift the  
388 equilibrium to the right in equation (5). Additionally, higher ionic strength also corresponds to an  
389 increased concentration of electrolytes in the aqueous phase, which could hinder the dissociation  
390 of the peroxymonosulfurous acid and shift the equilibrium in equation (6) to the right. In recent  
391 work by Liu et al. (2020), the rate of S(IV) oxidation by H<sub>2</sub>O<sub>2</sub> can be enhanced by up to a factor  
392 of 50 in aerosol aqueous phase compared to that of dilute solution. The highest ionic strength at  
393 which such enhancement was measured for the H<sub>2</sub>O<sub>2</sub> oxidation pathway was 15 mol kg<sup>-1</sup> (Liu et  
394 al., 2020).

395 Whereas the above analysis is based on the assumption that all the chemistry occurs in the bulk  
396 component of the particle, it is also possible that some component of the reaction occurs at the gas-  
397 particle interface and the overall kinetics can be affected by interfacial characteristics. For example,  
398 an enhanced ionic strength in the aerosol phase can also impact the interfacial reaction mechanisms.  
399 Previous study has shown evidence that interfacial chemistry is important for SO<sub>2</sub> oxidation in the  
400 aerosol phase (Laskin et al., 2003). With higher ionic strength, anions partitioning to the air-liquid  
401 interface can promote the overall reaction kinetics via proton transfer and thus accelerate the  
402 interfacial chemistry (Knipping et al., 2000; Mishra et al., 2012; Mekic et al., 2018; Mekic et al.,  
403 2020; Wei et al., 2018; Ruiz-Lopez et al., 2020). In addition to the catalytic effects of protons  
404 indicated in Eqn.5-7, Hung et al. (2015, 2018) observed significant SO<sub>3</sub><sup>-</sup> signal at the acidic

405 microdroplet surface, which can promote sulfate formation via radical propagation chain initiated  
406 by surrounding radicals and molecular oxygen (Eqn. 8-11):



407  
408 where the hydroxy radical can potentially be produced from decomposition of the labile organic  
409 peroxide in our system (Tong et al., 2016). However, we cannot distinguish whether the interfacial  
410 protons promote sulfate formation by catalyze the peroxide S(IV) oxidation pathway or the sulfur  
411 radical pathway at the current stage. In the recent study by Wei et al. (2018), a pH gradient was  
412 observed for phosphate-buffered aerosol droplets with the proton accumulated at the interface.  
413 Base on the pH-dependent aqueous phase kinetics measured in our previous work (Wang et al.,  
414 2019), such interfacial proton accumulation could potentially explain the enhanced kinetics we  
415 observed for aerosol in the current study. However, the chemical compositions are quite different.  
416 While phosphate-buffered particles were studied in Wei et al. (2018), acidic ammonium sulfate  
417 aerosol was used in our study. Also, the particle size in Wei et al. (2018) is significantly larger (20  
418  $\mu\text{m}$ ) than what was studied in the current study (200 nm). Thus, it should be noted that there is no  
419 direct evidence from the current study showing the relationship between the interfacial properties  
420 and  $\gamma_{\text{SO}_2}$ , and future studies are warranted.

421 Therefore, while more studies are needed to clearly delineate the roles of ionic strength, interfacial  
422 activity, bulk reactivity, and particle phase state quantitatively, the enhancement of  $\text{SO}_2$  oxidation

423 kinetics by highly concentrated aerosol particles compared to dilute aqueous solutions are  
424 concluded to be large (factor of 15-50) for the experimental conditions in the current study.

425

### 426 **3.4 SO<sub>2</sub> uptake and aerosol pH**

427 As indicated by the proposed reaction mechanisms (Eqn. 5-7), protons are important reaction  
428 intermediates for this SO<sub>2</sub> oxidation pathway. Previously, the aqueous phase reaction rate  
429 constants between organic peroxides and dissolved SO<sub>2</sub> were measured to be pH dependent  
430 (Wang et al., 2019). Moreover, the dissolution equilibrium of SO<sub>2</sub> into aqueous phase is also pH  
431 sensitive (Seinfeld and Pandis, 2012). Besides, many studies have shown that the uptake kinetics  
432 for gaseous species can be affected by the condensed phase pH (Shi et al., 1999; Gaston et al.,  
433 2014; Drozd et al., 2013; Jang and Kamens, 2001; Liu et al., 2015). Reactive uptake of ammonia  
434 was observed to depend on condensed phase acidity (Shi et al., 1999). Heterogeneous  
435 condensation of isoprene-derived epoxydiol onto seed aerosol was found to increase with proton  
436 concentration (Gaston et al., 2014). In the current study, the potential impact from particle phase  
437 pH on  $\gamma_{\text{SO}_2}$  was explored by adding HCl into the atomizing solution. To estimate the particle  
438 phase pH, two different methods associated with two different assumptions were used. In the  
439 first scenario, the aerosol pH in each experiment was estimated using the E-AIM III model  
440 (Clegg et al., 1998) based on the initial molar ratios of inorganic species (H<sup>+</sup>, NH<sub>4</sub><sup>+</sup>, SO<sub>4</sub><sup>2-</sup>, Cl<sup>-</sup>) in  
441 the atomizing solution and measured RH (around 50%). In the second scenario, the additional  
442 sulfate formed from reactive uptake of SO<sub>2</sub> was taken into consideration. The partitioning of HCl  
443 was allowed in the model simulation for both scenarios. The formation of sulfate would enhance  
444 the proton concentration in the aerosol liquid phase thus lower the aerosol pH. The average pH  
445 during the SO<sub>2</sub> uptake process is likely in between these two extremes.

446 Fig. 5 shows the measured reactive uptake coefficients of SO<sub>2</sub> as a function of the calculated pH.  
447 The reactive uptake coefficient was found to weakly increase with decreasing pH, which is  
448 consistent with acid-catalyzed reactions between peroxides and dissolved SO<sub>2</sub> as measured in the  
449 bulk phase (Lind et al., 1987; Wang et al., 2019).  $\gamma_{\text{SO}_2}$  was also predicted for the same range of  
450 pH based on Eqn. 4 and the pH-dependent bulk-phase reaction rate constants measured  
451 previously (Wang et al., 2019). Indicated by Fig. 5, the measured  $\gamma_{\text{SO}_2}$  again exceeds the  
452 predicted  $\gamma_{\text{SO}_2}$  by about a factor of 50, which is consistent with what we reported earlier and is  
453 likely due to the effects of aerosol ionic strength.

454 Unlike the observed  $\gamma_{\text{SO}_2}$ , however, the predicted  $\gamma_{\text{SO}_2}$  does not exhibit a monotonic trend.  $\gamma_{\text{SO}_2}$  is  
455 expected to decrease with decreasing pH at high pH (>2) as the effective Henry's law constant of  
456 SO<sub>2</sub> decreases with higher acidity (Seinfeld and Pandis, 2012).  $\gamma_{\text{SO}_2}$  is not expected to increase  
457 with decreasing pH until pH is below 2 where the acidity enhancement in reaction rate constant  
458 exceeds the decrease in SO<sub>2</sub> solubility. As illustrated earlier, extrapolating dilute aqueous-phase  
459 kinetics to the highly concentrated aerosol requires considering effects from high solute strength.  
460 Solute strength may change the pH dependence of  $\gamma_{\text{SO}_2}$  in two ways. First, the solubility of SO<sub>2</sub>  
461 may decrease and become less dependent on pH as ionic strength increases (Rodríguez-Sevilla et  
462 al., 2002). A former study (Leng et al., 2015) has shown that the effective Henry's law of  
463 triethylamine decreases with increased ionic strength. Another potential explanation is that the  
464 aqueous phase reaction rate constant can be more pH-dependent at high ionic strengths than what  
465 we measured previously in dilute solutions. In either case, the inflection of the predicted  $\gamma_{\text{SO}_2}$   
466 would change and  $\gamma_{\text{SO}_2}$  could become more negatively dependent on pH ( $d[\gamma_{\text{SO}_2}]/d[\text{pH}]$  becomes  
467 less positive in the high pH range and/or more negative in the low pH range), which would  
468 match more closely with the observed dependence. It should also be noted that there are

469 substantial uncertainties in estimating pH values, originating from the partitioning of organics,  
470 organic-inorganic phase separations, mixing state of specific ions, uncertain activity coefficients  
471 and the propagation of RH uncertainties (Clegg et al., 2008; Fountoukis et al., 2009; Guo et al.,  
472 2016). Also, the reactive uptake is a dynamic process and will influence aerosol pH in turn upon  
473 sulfate formation. In summary, while the magnitude of predicted  $\gamma_{\text{SO}_2}$  is consistent with our  
474 expected values (after accounting for the enhancement by high aerosol solute strength), we  
475 cannot fully explain the dependence of  $\gamma_{\text{SO}_2}$  on aerosol pH at the current stage. Future studies  
476 should investigate how the effective Henry's law of  $\text{SO}_2$  and pH dependence of reaction rate  
477 constants vary in aerosol liquid phase with high solute strength in order to have a more  
478 comprehensive understanding of the relationship between  $\gamma_{\text{SO}_2}$  and aerosol pH.

479

### 480 **3.4 SO<sub>2</sub> uptake onto SOA**

481  $\gamma_{\text{SO}_2}$  was measured for a few model SOA systems, as organic peroxides are abundant in SOA  
482 (Surratt et al., 2006;Kautzman et al., 2009;Krapf et al., 2016;Bonn et al., 2004). Here we studied  
483 SOA formed from monoterpene ozonolysis and toluene photooxidation. It should be noted that  
484 for the  $\gamma_{\text{SO}_2}$  measurements of toluene SOA, a strong hydrocarbon interference was observed with  
485 the  $\text{SO}_2$  analyzer, likely stemming from the high concentrations of gas-phase aromatic  
486 compounds. A rough estimate of the uptake rate for toluene SOA from aerosol mass  
487 spectrometer sulfate measurements is provided in the SI (Section 1). The reactive uptake  
488 coefficient of  $\text{SO}_2$  onto Saharan mineral dust was reported on the order of  $10^{-5}$  (Adams et al.,  
489 2005).  $\gamma_{\text{SO}_2}$  onto dust with the coexistence of  $\text{NO}_2$  and  $\text{NH}_3$  under various RH conditions were  
490 measured to be  $10^{-7}$  to  $10^{-5}$  (Zhang et al., 2019). For a variety of metal oxides,  $\text{SO}_2$  reactive  
491 uptake coefficients were quantified to be between  $10^{-6}$  and  $10^{-4}$  (Usher et al., 2002; Fu et al.,

492 2007; Shang et al., 2010). More recently,  $\gamma_{\text{SO}_2}$  studied for heterogeneous sulfate formation by  
493 photolysis of particulate nitrate were reported in the range of  $10^{-6}$  to  $10^{-5}$  (Gen et al., 2019). As  
494 shown in Fig. 6,  $\gamma_{\text{SO}_2}$  for all SOA systems were measured to be on the order of  $10^{-4}$ . Similar  $\gamma_{\text{SO}_2}$   
495 values on the order of  $10^{-4}$  were measured for  $\alpha$ -pinene SOA by Yao et al. (2019), and  $10^{-5}$  for  
496 limonene SOA estimated from the chamber study by Ye et al. (2018). The reaction products  
497 from this SOA and  $\text{SO}_2$  interaction will be reported in a separate study.

498

#### 499 **4. Atmospheric Implications**

500 Oxidation of atmospheric hydrocarbons produces reactive intermediates that can potentially  
501 interact with  $\text{SO}_2$  and form particulate sulfate, contributing to PM formation and growth (Berndt  
502 et al., 2015; Mauldin et al., 2012; Yao et al., 2019). Organic peroxides generated from both  
503 biogenic and anthropogenic hydrocarbon emissions are abundant in submicron aerosol. Given  
504 that they are highly reactive with relatively short lifetimes (Bonn et al., 2004; Krapf et al.,  
505 2016; Qiu et al., 2020), these species could serve as important condensed phase oxidants for gas  
506 phase  $\text{SO}_2$ . Combining laboratory measurements and model predictions, the current study  
507 investigated heterogeneous reactions between  $\text{SO}_2$  and particulate organic peroxide. The  
508 measured  $\gamma_{\text{SO}_2}$  for organic peroxide containing aerosol ranges from  $10^{-5}$  to  $10^{-2}$  in this study.  
509 Based on the modeling work by Wang et al. (2014), adding an  $\text{SO}_2$  uptake pathway to GEOS-  
510 Chem with a reactive uptake coefficient of  $10^{-4}$  could improve the surface sulfate prediction by  
511 more than 50% during a severe haze episode over North China (RH 50%), suggesting the  
512 potential importance of this multiphase reaction pathway, especially when SOA is the dominant  
513 component in particulate matter.

514 The dependence of the heterogeneous kinetics on RH, aerosol pH, peroxide type, and peroxide  
515 content were also evaluated. The experimentally measured  $\gamma_{\text{SO}_2}$  was found to be consistently  
516 higher than that predicted from reaction kinetics with organic peroxides in the dilute aqueous  
517 phase. This discrepancy can be potentially explained by the effects of high ionic strength  
518 presented in the aerosol, suggesting that the impact from highly concentrated solutes needs to be  
519 taken into consideration when applying aqueous phase kinetics to aerosol multiphase chemistry,  
520 especially for particles containing strong electrolytes. We also observed that the kinetics of this  
521 multiphase reaction exhibit a weak dependence on pH. Increasing the condensed-phase acidity  
522 may enhance the heterogeneous rate constant at low pH, and while this pH dependence is  
523 consistent with that of the aqueous phase reaction rate constant measured previously, it is not  
524 consistent with the decrease of effective Henry's law constant of  $\text{SO}_2$  along with enhanced  
525 acidity. Also, it is likely that within the uncertainties, there may not be an observable  $\gamma_{\text{SO}_2}$ -pH  
526 trend. Currently, we are not able to fully explain the pH dependence, and further studies are  
527 warranted. Particle phase peroxide content was observed to be linearly correlated with  $\gamma_{\text{SO}_2}$ .  
528 Moreover,  $\gamma_{\text{SO}_2}$  measured for 2-butanone peroxide was found to be orders of magnitude higher  
529 than that of cumene hydroperoxide and tert-butyl hydroperoxide. The difference in  $\gamma_{\text{SO}_2}$  among  
530 various types of organic peroxides can be partially explained by their condensed-phase reactivity  
531 and gas-particle partitioning.

532 In general, we found the observed  $\gamma_{\text{SO}_2}$  in this study can be summarized using the following  
533 semiempirical multilinear relationship:

$$534 \quad \log \gamma = -1.7 + 0.0024 \times k'' + 0.46 \times PAS + 0.024 \times RH - 1.9 \times Vp \quad (8)$$

535 where  $\gamma$  is the reactive uptake coefficient,  $k''$  is the aqueous phase S(IV) oxidation rate constant  
536 ( $\text{M}^{-1} \text{s}^{-1}$ ),  $PAS$  is the molar ratio between particulate peroxide and ammonium sulfate in the



537 atomizing solution, which is a proxy for the amount of peroxide in both gas and particle phases  
538 applied in the current study,  $RH$  is the relative humidity (%),  $Vp$  is the vapour pressure (kPa) of  
539 the peroxide. Fig. 7 illustrates the degree to which this semi-empirical expression describes the  
540 experimental data for ammonium sulfate aerosol mixed with the three types of organic peroxides.  
541 Residual evaluations of this multilinear regression can be found Fig. S9. We caution that this  
542 equation is not directly applicable to atmospheric models in its current form, especially since the  
543 particle phase peroxide content (PAS) value we applied as input is a calculated value, rather than  
544 a measurement. However, it illustrates the internal consistency of our experimental results across  
545 a range of  $RH$ , peroxide content, and aqueous phase reactivities, which are the key variables for  
546 uptake rates. Better understanding of ionic strengths and pH in aerosol, either through modeling  
547 or direct measurements of these variables, is needed to establish the coefficient dependence.  
548 Future studies should be focused on exploring  $\gamma_{SO_2}$  and the reaction products for various types of  
549 SOA as well as ambient particles under atmospherically relevant conditions, evaluating the  
550 underlying impacts from photochemical condition, chemical composition, particle morphology,  
551 ionic strength and interfacial properties on this multiphase physicochemical process. Overall,  
552  $\gamma_{SO_2}$  presented in our study and its relationship with ambient  $RH$ , aerosol pH, ionic strength,  
553 particulate peroxide content and type could provide a framework for the implementation of this  
554 heterogeneous mechanism in atmospheric models to have a better understanding of ambient  
555 sulfate formation and particle growth.

556

557

558

559

560 *Author contributions*

561 A.W.H. C. and S.W. designed the study. S.W., T. L., and J. J. performed the experiments. S.W.,  
562 A.W.H. C., T. L., and J. J. analyzed data. S.W. and A.W.H. C. wrote the manuscript with the  
563 input from all co-authors.

564

565 *Data availability*

566 All data presented in this study are available in the supplemental material and have been  
567 deposited in figshare.

568

569 *Associated content*

570 Supporting Information.

571

572 *Competing interests*

573 The authors declare no competing financial interest.

574

575 *Acknowledgements*

576 This work was supported by Natural Sciences and Engineering Research Council Discovery Grant.

577 The authors would like to thank Dr. Greg Evans, Dr. Yue Zhao and Dr. Christopher Lim for helpful  
578 comments and discussions. Special thanks to SOCAAR for providing the SO<sub>2</sub> analyzer.

579

580

581

582

583

584 **Reference**

- 585 Abbatt, J. P. D., Lee, A. K. Y., and Thornton, J. A.: Quantifying trace gas uptake to tropospheric  
586 aerosol: recent advances and remaining challenges, *Chem. Soc. Rev.*, 41, 6555–6581,  
587 <https://doi.org/10.1039/c2cs35052a>, 2012.
- 588 Adams, J. W., Rodriguez, D., and Cox, R. A.: The uptake of SO<sub>2</sub> on Saharan dust: a flow tube  
589 study, *Atmos. Chem. Phys.*, 5, 2643–2676, doi:10.5194/acp-5-2643-2005, 2005.
- 590 Andreae, M.O., Afchine, A., Albrecht, R., Holanda, B.A., Artaxo, P., Barbosa, H.M., Borrmann,  
591 S., Cecchini, M.A., Costa, A., Dollner, M. and Fütterer, D.: Aerosol characteristics and particle  
592 production in the upper troposphere over the Amazon Basin, *Atmos. Chem. Phys.*, 18, 921–961,  
593 2018.
- 594 Atkinson, R., and Arey, J.: Atmospheric degradation of volatile organic compounds, *Chem.*  
595 *Rev.*, 103, 4605-4638, 2003.
- 596 Berndt, T., Richters, S., Kaethner, R., Voigtländer, J., Stratmann, F., Sipilä, M., Kulmala, M.,  
597 and Herrmann, H.: Gas-phase ozonolysis of cycloalkenes: Formation of highly oxidized RO<sub>2</sub>  
598 radicals and their reactions with NO, NO<sub>2</sub>, SO<sub>2</sub>, and other RO<sub>2</sub> radicals, *J. Phys. Chem. A*, 119,  
599 10336-10348, 10.1021/acs.jpca.5b07295, 2015.
- 600 Bianchi, F., Kurtén, T., Riva, M., Mohr, C., Rissanen, M. P., Roldin, P., Berndt, T., Crouse, J.  
601 D., Wennberg, P. O., Mentel, T. F., Wildt, J., Junninen, H., Jokinen, T., Kulmala, M., Worsnop,  
602 D. R., Thornton, J. A., Donahue, N., Kjaergaard, H. G., and Ehn, M.: Highly oxygenated organic  
603 molecules (HOM) from gas-phase autoxidation involving peroxy radicals: A key contributor to  
604 atmospheric aerosol, *Chem. Rev.*, 119, 3472-3509, 10.1021/acs.chemrev.8b00395, 2019.
- 605 Bonn, B., von Kuhlmann, R., and Lawrence, M. G.: High contribution of biogenic  
606 hydroperoxides to secondary organic aerosol formation, *Geophys. Res. Lett.*, 31, L10108,  
607 <https://doi.org/10.1029/2003GL019172>, 2004.
- 608 Chen, Q., Farmer, D. K., Schneider, J., Zorn, S. R., Heald, C. L., Karl, T. G., Guenther, A.,  
609 Allan, J. D., Robinson, N., Coe, H., Kimmel, J. R., Pauliquevis, T., Borrmann, S., Pöschl, U.,  
610 Andreae, M. O., Artaxo, P., Jimenez, J. L., and Martin, S. T.: Mass spectral characterization of  
611 submicron biogenic organic particles in the Amazon Basin, *Geophys. Res. Lett.*, 36, L20806,  
612 <https://doi.org/10.1029/2009GL039880>, 2009.
- 613 Chen, T., Chu, B., Ge, Y., Zhang, S., Ma, Q., He, H., and Li, S.-M.: Enhancement of aqueous  
614 sulfate formation by the coexistence of NO<sub>2</sub>/NH<sub>3</sub> under high ionic strengths in aerosol water,  
615 *Environ. Pollut.*, 252, 236-244, <https://doi.org/10.1016/j.envpol.2019.05.119>, 2019.
- 616 Cheng, Y., Su, H., Koop, T., Mikhailov, E., and Pöschl, U.: Size dependence of phase transitions  
617 in aerosol nanoparticles, *Nat. Commun.*, 6, 5923, 10.1038/ncomms6923, 2015.
- 618 Cheng, Y. F., Zheng, G. J., Wei, C., Mu, Q., Zheng, B., Wang, Z. B., Gao, M., Zhang, Q., He, K.  
619 B., Carmichael, G., Pöschl, U., and Su, H.: Reactive nitrogen chemistry in aerosol water as a  
620 source of sulfate during haze events in China, *Sci. Adv.*, 2, e1601530, [https://doi.org/10.1126/](https://doi.org/10.1126/sciadv.1601530)  
621 [sciadv.1601530](https://doi.org/10.1126/sciadv.1601530), 2016.

622 Ciobanu, V. G., Marcolli, C., Krieger, U. K., Weers, U., and Peter, T.: Liquid-liquid phase  
623 separation in mixed organic/inorganic aerosol particles, *J. Phys. Chem. A*, 113, 10966–10978,  
624 2009.

625 Clegg, S. L., Brimblecombe, P., and Wexler, A. S.: Thermodynamic model of the system  
626  $\text{H}^+ - \text{NH}_4^+ - \text{Na}^+ - \text{SO}_4^{2-} - \text{NO}_3^- - \text{Cl}^- - \text{H}_2\text{O}$  at 298.15 K, *J. Phys. Chem. A*, 102, 2155–2171,  
627 <https://doi.org/10.1021/jp973043j>, 1998.

628 Clegg, S. L., Kleeman, M. J., Griffin, R. J., and Seinfeld, J. H.: Effects of uncertainties in the  
629 thermodynamic properties of aerosol components in an air quality model – Part 1: Treatment of  
630 inorganic electrolytes and organic compounds in the condensed phase, *Atmos. Chem. Phys.*, 8,  
631 1057–1085, <http://www.atmos-chem-phys.net/8/1057/2008/>, 2008.

632 Docherty, K. S., Wu, W., Lim, Y. B., and Ziemann, P. J.: Contributions of organic peroxides to  
633 secondary aerosol formed from reactions of monoterpenes with  $\text{O}_3$ , *Environ. Sci. Technol.*, 39,  
634 4049–4059, 2005.

635 Dovrou, E., Rivera-Rios, J. C., Bates, K. H., and Keutsch, F. N.: Sulfate formation via cloud  
636 processing from isoprene hydroxyl hydroperoxides (ISOPOOH), *Environ. Sci. Technol.*, 53,  
637 12476–12484, [10.1021/acs.est.9b04645](https://doi.org/10.1021/acs.est.9b04645), 2019.

638 Drozd, G. T., Woo, J. L., and McNeill, V. F.: Self-limited uptake of  $\alpha$ -pinene oxide to acidic  
639 aerosol: the effects of liquid-liquid phase separation and implications for the formation of  
640 secondary organic aerosol and organosulfates from epoxides, *Atmos. Chem. Phys.*, 13, 8255–  
641 8263, [doi:10.5194/acp-13-8255-2013](https://doi.org/10.5194/acp-13-8255-2013), 2013.

642 Epstein, S. A., Blair, S. L., and Nizkorodov, S. A.: Direct photolysis of  $\alpha$ -pinene ozonolysis  
643 secondary organic aerosol: effect on particle mass and peroxide content, *Environ. Sci. Technol.*,  
644 48, 11251–11258, 2014.

645 Fairlie, T. D., Jacob, D. J., Dibb, J. E., Alexander, B., Avery, M. A., van Donkelaar, A., and  
646 Zhang, L.: Impact of mineral dust on nitrate, sulfate, and ozone in transpacific Asian pollution  
647 plumes, *Atmos. Chem. Phys.*, 10, 3999–4012, [doi:10.5194/acp-10-3999-2010](https://doi.org/10.5194/acp-10-3999-2010), 2010.

648 Fountoukis, C., Nenes, A., Sullivan, A., Weber, R., Van Reken, T., Fischer, M., Matas, E.,  
649 Moya, M., Farmer, D., and Cohen, R. C.: Thermodynamic characterization of Mexico City  
650 aerosol during MILAGRO 2006, *Atmos. Chem. Phys.*, 9, 2141–2156, [http://www.atmos-chem-](http://www.atmos-chem-phys.net/9/2141/2009/)  
651 [phys.net/9/2141/2009/](http://www.atmos-chem-phys.net/9/2141/2009/), 2009.

652 Freedman, M. A.: Phase separation in organic aerosol, *Chem. Soc. Rev.*, 46, 7694–7705,  
653 <https://doi.org/10.1039/C6CS00783J>, 2017.

654 Fu, H. B., Wang, X., Wu, H. B., Yin, Y., and Chen, J. M.: Heterogeneous uptake and oxidation  
655 of  $\text{SO}_2$  on iron oxides, *J. Phys. Chem. C*, 111, 6077–6085, 2007.

656 Gao, M., Carmichael, G. R., Wang, Y., Saide, P. E., Yu, M., Xin, J., Liu, Z., and Wang, Z.:  
657 Modeling study of the 2010 regional haze event in the North China Plain, *Atmos. Chem. Phys.*,  
658 16, 1673–1691, <https://doi.org/10.5194/acp-16-1673-2016>, 2016.

659 Gaston, C. J., Riedel, T. P., Zhang, Z., Gold, A., Surratt, J. D., and Thornton, J. A.: Reactive  
660 uptake of an isoprene-derived epoxydiol to submicron aerosol particles, *Environ. Sci. Technol.*,  
661 48, 11178–11186, [10.1021/es5034266](https://doi.org/10.1021/es5034266), 2014.

662 Gen, M., Zhang, R., Huang, D. D., Li, Y., and Chan, C. K.: Heterogeneous SO<sub>2</sub> oxidation in  
663 sulfate formation by photolysis of particulate nitrate, *Environ. Sci. Tech. Lett.*, 6, 86–91,  
664 <https://doi.org/10.1021/acs.estlett.8b00681>, 2019.

665 Griffiths, P. T., Badger, C. L., Cox, R. A., Folkers, M., Henk, H. H., and Mentel, T. F.: Reactive  
666 uptake of N<sub>2</sub>O<sub>5</sub> by aerosols containing dicarboxylic acids. Effect of particle phase, composition,  
667 and nitrate content, *J. Phys. Chem. A*, 113, 5082–5090, [10.1021/jp8096814](https://doi.org/10.1021/jp8096814), 2009.

668 Gunz, D. W. and Hoffmann, M. R.: Atmospheric chemistry of peroxides: A review, *Atmos.*  
669 *Environ.*, 24A, 1601–1633, [https://doi.org/10.1016/0960-1686\(90\)90496-A](https://doi.org/10.1016/0960-1686(90)90496-A), 1990.

670 Guo, H., Sullivan, A. P., Campuzano-Jost, P., Schroder, J. C., LopezHilfiker, F. D., Dibb, J. E.,  
671 Jimenez, J. L., Thornton, J. A., Brown, S. S., Nenes, A., and Weber, R. J.: Fine particle pH  
672 and the partitioning of nitric acid during winter in the northeastern United States, *J. Geophys.*  
673 *Res. Atmos.*, 121, 10355–10376, <https://doi.org/10.1002/2016JD025311>, 2016.

674 Guo, H., Weber, R. J., and Nenes, A.: High levels of ammonia do not raise fine particle pH  
675 sufficiently to yield nitrogen oxide-dominated sulfate production, *Sci. Rep.*, 7, 12109, 2017.

676 Hallquist, M., Wenger, J. C., Baltensperger, U., Rudich, Y., Simpson, D., Claeys, M., Dommen,  
677 J., Donahue, N. M., George, C., Goldstein, A. H., Hamilton, J. F., Herrmann, H., Hoffmann, T.,  
678 Iinuma, Y., Jang, M., Jenkin, M. E., Jimenez, J. L., Kiendler-Scharr, A., Maenhaut, W.,  
679 McFiggans, G., Mentel, Th. F., Monod, A., Prévôt, A. S. H., Seinfeld, J. H., Surratt, J. D.,  
680 Szmigielski, R., and Wildt, J.: The formation, properties and impact of secondary organic  
681 aerosol: current and emerging issues, *Atmos. Chem. Phys.*, 9, 5155–5236, <https://doi.org/10.5194/acp9-5155-2009>, 2009.

682  
683 Halperin, J., and Taube, H.: The transfer of oxygen atoms in oxidation—reduction reactions. IV.  
684 The reaction of hydrogen peroxide with sulfite and thiosulfate, and of oxygen, manganese  
685 dioxide and of permanganate with sulfite, *J. Am. Chem. Soc.*, 74, 380–382, 1952.

686 Hanson, D. R., Ravishankara, A. R., and Solomon, S.: Heterogeneous reactions in sulfuric acid  
687 aerosols: A framework for model calculations, *J. Geophys. Res.*, 99, 3615, <https://doi.org/10.1029/93JD02932>, 1994.

688  
689 Hartz, K. E. H., Rosenorn, T., Ferchak, S. R., Raymond, T. M., Bilde, M., Donahue, N. M., and  
690 Pandis, S. N.: Cloud condensation nuclei activation of monoterpene and sesquiterpene  
691 secondary organic aerosol, *J. Geophys. Res.-Atmos.*, 110(D14), D14208, [doi:10.1029/2004J](https://doi.org/10.1029/2004JD005754)  
692 [D005754](https://doi.org/10.1029/2004JD005754), 2005.

693 He, L.-Y., Huang, X.-F., Xue, L., Hu, M., Lin, Y., Zheng, J., Zhang, R., and Zhang, Y.-H.:  
694 Submicron aerosol analysis and organic source apportionment in an urban atmosphere  
695 in Pearl River Delta of China using high-resolution aerosol mass spectrometry, *J. Geophys. Res.*  
696 *Atmos.*, 116, D12304, <https://doi.org/10.1029/2010JD014566>, 2011.

697 Herrmann, H.: Kinetics of aqueous phase reactions relevant for atmospheric chemistry, *Chem.*  
698 *Rev.*, 103, 4691–4716, 2003.

699 Hildebrandt, L., Donahue, N. M., Pandis, S. N.: High formation of secondary organic aerosol  
700 from the photo-oxidation of toluene, *Atmos. Chem. Phys.*, 9, 2973–2986, <https://doi.org/10.5194/acp-9-2973-2009>, 2009.

701

702 Huang, L., An, J., Koo, B., Yarwood, G., Yan, R., Wang, Y., Huang, C., and Li, L.: Sulfate  
703 formation during heavy winter haze events and the potential contribution from heterogeneous  
704 SO<sub>2</sub> + NO<sub>2</sub> reactions in the Yangtze River Delta region, China, *Atmos. Chem. Phys.*, 19, 14311-  
705 14328, 10.5194/acp-19-14311-2019, 2019.

706 Huang, L., Coddens, E. M., and Grassian, V. H.: Formation of organosulfur compounds from  
707 aqueous phase reactions of S (IV) with methacrolein and methyl vinyl ketone in the presence of  
708 transition metal ions, *ACS Earth Space Chem.*, 3, 1749-1755, 2019.

709 Huang, L., Liu, T. and Grassian, V. H.: Radical-initiated formation of aromatic organosulfates  
710 and sulfonates in the aqueous phase. *Environ. Sci. Technol.*, 54, 11857–11864,  
711 <https://doi.org/10.1021/acs.est.0c05644>, 2020.

712 Huang, R. J., Zhang, Y. L., Bozzetti, C., Ho, K. F., Cao, J. J., Han, Y. M., Daellenbach, K. R.,  
713 Slowik, J. G., Platt, S. M., Canonaco, F., Zotter, P., Wolf, R., Pieber, S. M., Brun, E. A., Crippa,  
714 M., Ciarelli, G., Piazzalunga, A., Schwikowski, M., Abbaszade, G., Schnelle-Kreis, J.,  
715 Zimmermann, R., An, Z., Szidat, S., Baltensperger, U., Haddad, I. E., and Prevot, A. S. H.: High  
716 secondary aerosol contribution to particulate pollution during haze events in China, *Nature*, 514,  
717 218–222, 2014.

718 Huang, R. J., He, Y., Duan, J., Li, Y., Chen, Q., Zheng, Y., Chen, Y., Hu, W., Lin, C., Ni, H.,  
719 Dai, W., Cao, J., Wu, Y., Zhang, R., Xu, W., Ovadnevaite, J., Ceburnis, D., Hoffmann, T., and  
720 O'Dowd, C. D.: Contrasting sources and processes of particulate species in haze days with low  
721 and high relative humidity in wintertime Beijing, *Atmos. Chem. Phys.*, 20, 9101-9114,  
722 10.5194/acp-20-9101-2020, 2020.

723 Hung, H. M. and Hoffmann, M. R.: Oxidation of gas-phase SO<sub>2</sub> on the surfaces of acidic  
724 microdroplets: Implications for sulfate and sulfate radical anion formation in the atmospheric  
725 liquid phase, *Environ. Sci. Technol.*, 49, 13768–13776, <https://doi.org/10.1021/acs.est.5b01658>,  
726 2015.

727 Hung, H. M., Hsu, M. N., and Hoffmann, M. R.: Quantification of SO<sub>2</sub> oxidation on interfacial  
728 surfaces of acidic micro-droplets: Implication for ambient sulfate formation, *Environ. Sci.*  
729 *Technol.*, 52, 9079–9086, <https://doi.org/10.1021/acs.est.8b01391>, 2018.

730 Jang, M., and Kamens, R. M.: Atmospheric secondary aerosol formation by heterogeneous  
731 reactions of aldehydes in the presence of a sulfuric acid aerosol catalyst, *Environ. Sci. Technol.*,  
732 35, 4758-4766, 10.1021/es010790s, 2001.

733 Jimenez, J. L., Canagaratna, M. R., Donahue, N. M., Prevot, A. S. H., Zhang, Q., Kroll, J. H.,  
734 DeCarlo, P. F., Allan, J. D., Coe, H., Ng, N. L., Aiken, A. C., Docherty, K. S., Ulbrich, I. M.,  
735 Grieshop, A. P., Robinson, A. L., Duplissy, J., Smith, J. D., Wilson, K. R., Lanz, V. A., Hueglin,  
736 C., Sun, Y. L., Tian, J., Laaksonen, A., Raatikainen, T., Rautiainen, J., Vaattovaara, P., Ehn, M.,  
737 Kulmala, M., Tomlinson, J. M., Collins, D. R., Cubison, M. J., Dunlea, J., Huffman, J. A.,  
738 Onasch, T. B., Alfarra, M. R., Williams, P. I., Bower, K., Kondo, Y., Schneider, J., Drewnick,  
739 F., Borrmann, S., Weimer, S., Demerjian, K., Salcedo, D., Cottrell, L., Griffin, R., Takami, A.,  
740 Miyoshi, T., Hatakeyama, S., Shimono, A., Sun, J. Y., Zhang, Y. M., Dzepina, K., Kimmel,  
741 J. R., Sueper, D., Jayne, J. T., Herndon, S. C., Trimborn, A. M., Williams, L. R., Wood, E. C.,  
742 Middlebrook, A. M., Kolb, C. E., Baltensperger, U., and Worsnop, D. R.: Evolution of organic  
743 aerosols in the atmosphere, *Science*, 326, 1525–1529, <https://doi.org/10.1126/science.1180353>,  
744 2009.

745 Kautzman, K., Surratt, J., Chan, M., Chan, A., Hersey, S., Chhabra, P., Dalleska, N., Wennberg,  
746 P., Flagan, R., and Seinfeld, J.: Chemical composition of gas-and aerosol-phase products from  
747 the photooxidation of naphthalene, *J. Phys. Chem. A*, 114, 913-934, 2009.

748 Knipping, E. M., Lakin, M. J., Foster, K. L., Jungwirth, P., Tobias, D. J., Gerber, R. B., Dabdub,  
749 D., and Finlayson-Pitts, B. J.: Experiments and simulations of ion-enhanced interfacial chemistry  
750 on aqueous NaCl aerosols, *Science*, 288, 301, 10.1126/science.288.5464.301, 2000.

751 Krapf, M., El Haddad, I., Bruns, E. A., Molteni, U., Daellenbach, K. R., Prévôt, A. S.,  
752 Baltensperger, U., and Dommen, J.: Labile peroxides in secondary organic aerosol, *Chem*, 1,  
753 603-616, 2016.

754 Laskin, A., Gaspar, D. J., Wang, W., Hunt, S. W., Cowin, J. P., Colson, S. D., and Finlayson-  
755 Pitts, B. J.: Reactions at interfaces as a source of sulfate formation in sea-salt particles, *Science*,  
756 301, 340, 10.1126/science.1085374, 2003.

757 Leng, C. B., Roberts, J. E., Zeng, G., Zhang, Y. H., and Liu, Y.: Effects of temperature, pH, and  
758 ionic strength on the Henry's law constant of triethylamine, *Geophys. Res. Lett.*, 42, 3569-3575,  
759 10.1002/2015gl063840, 2015.

760 Li, G., Bei, N., Cao, J., Huang, R., Wu, J., Feng, T., Wang, Y., Liu, S., Zhang, Q., Tie, X., and  
761 Molina, L. T.: A possible pathway for rapid growth of sulfate during haze days in China, *Atmos.*  
762 *Chem. Phys.*, 17, 3301–3316, <https://doi.org/10.5194/acp17-3301-2017>, 2017.

763 Li, J., Zhang, Y., Cao, F., Zhang, W., Fan, M., Lee, X., Michalski, G.: Stable sulfur isotopes  
764 revealed a major role of transition-metal-ion catalyzed SO<sub>2</sub> oxidation in haze episodes,  
765 doi:10.1021/acs.est.9b07150, 2020.

766 Lind, J. A., Lazrus, A. L., and Kok, G. L.: Aqueous phase oxidation of sulfur (IV) by hydrogen  
767 peroxide, methylhydroperoxide, and peroxyacetic acid, *J. Geophys. Res. Atmos.*, 92, 4171-4177,  
768 1987.

769 Liu, C., Chen, T., Liu, Y., Liu, J., He, H., Zhang, P.: Enhancement of secondary organic aerosol  
770 formation and its oxidation state by SO<sub>2</sub> during photooxidation of 2-methoxyphenol, *Atmos.*  
771 *Chem. Phys.*, 19, 2687-2700, 2019.

772 Liu, L., Bei, N., Wu, J., Liu, S., Zhou, J., Li, X., Yang, Q., Feng, T., Cao, J., Tie, X. and Li, G.:  
773 Effects of stabilized Criegee intermediates (sCIs) on sulfate formation: a sensitivity analysis  
774 during summertime in Beijing–Tianjin–Hebei (BTH), China, *Atmos. Chem. Phys.*, 19, 13341-  
775 13354, 2019.

776 Liu, T., Clegg, S. L. and Abbatt, J. P. D.: Fast oxidation of sulfur dioxide by hydrogen peroxide  
777 in deliquesced aerosol particles, *Proc. Natl. Acad. Sci. U. S. A.*, 117, 1354–1359, 2020.

778 Liu, Y., Liggió, J., Staebler, R., and Li, S. M.: Reactive uptake of ammonia to secondary organic  
779 aerosols: kinetics of organonitrogen formation, *Atmos. Chem. Phys.*, 15, 13569–13584,  
780 doi:10.5194/acp-15-13569-2015, 2015.

781 Maaß, F., Elias, H., and Wannowius, K. J.: Kinetics of the oxidation of hydrogen sulfite by  
782 hydrogen peroxide in aqueous solution: ionic strength effects and temperature dependence,  
783 *Atmos. Environ.*, 33, 4413-4419, [https://doi.org/10.1016/S1352-2310\(99\)00212-5](https://doi.org/10.1016/S1352-2310(99)00212-5), 1999.

784 Mauldin, R. L., Berndt, T., Sipilä, M., Paasonen, P., Petäjä, T., Kim, S., Kurtén, T., Stratmann,  
785 F., Kerminen, V. M., and Kulmala, M.: A new atmospherically relevant oxidant of sulphur  
786 dioxide, *Nature*, 488, 193–196, <https://doi.org/10.1038/nature11278>, 2012.

787 Mekic, M., Loisel, G., Zhou, W., Jiang, B., Vione, D., and Gligorovski, S.: Ionic-strength effects  
788 on the reactive uptake of ozone on aqueous pyruvic acid: Implications for air–sea ozone  
789 deposition, *Environ. Sci. Technol.*, 52, 12306–12315, [10.1021/acs.est.8b03196](https://doi.org/10.1021/acs.est.8b03196), 2018.

790 Mekic, M., Zeng, J., Zhou, W., Loisel, G., Jin, B., Li, X., Vione, D., and Gligorovski, S.: Ionic  
791 strength effect on photochemistry of fluorene and dimethylsulfoxide at the air–sea interface:  
792 Alternative formation pathway of organic sulfur compounds in a marine atmosphere, *ACS Earth  
793 Space Chem.*, 4, 1029–1038, [10.1021/acsearthspacechem.0c00059](https://doi.org/10.1021/acsearthspacechem.0c00059), 2020.

794 Mishra, H., Enami, S., Nielsen, R. J., Hoffmann, M. R., Goddard, W. A., and Colussi, A. J.:  
795 Anions dramatically enhance proton transfer through aqueous interfaces, *Proc. Natl. Acad. Sci.  
796 U. S. A.*, 109, 10228–10232, 2012.

797 Newland, M. J., Rickard, A. R., Vereecken, L., Muñoz, A., Ródenas, M., and Bloss, W. J.:  
798 Atmospheric isoprene ozonolysis: impacts of stabilised Criegee intermediate reactions with SO<sub>2</sub>,  
799 H<sub>2</sub>O and dimethyl sulfide, *Atmos. Chem. Phys.*, 15, 9521–9536, <https://doi.org/10.5194/acp-15-9521-2015>, 2015.

801 Ng, N., Kroll, J., Chan, A., Chhabra, P., Flagan, R., and Seinfeld, J.: Secondary organic aerosol  
802 formation from m-xylene, toluene, and benzene, *Atmos. Chem. Phys.*, 7, 3909–3922,  
803 <http://www.atmos-chem-phys.net/7/3909/2007/>, 2007.

804 Ng, N. L., Kwan, A. J., Surratt, J. D., Chan, A. W. H., Chhabra, P. S., Sorooshian, A., Pye, H. O.  
805 T., Crouse, J. D., Wennberg, P. O., Flagan, R. C., and Seinfeld, J. H.: Secondary organic  
806 aerosol (SOA) formation from reaction of isoprene with nitrate radicals (NO<sub>3</sub>), *Atmos. Chem.  
807 Phys.*, 8, 4117–4140, <http://www.atmos-chem-phys.net/8/4117/2008/>, 2008.

808 Nguyen, T. B., Tyndall, G. S., Crouse, J. D., Teng, A. P., Bates, K. H., Schwantes, R. H.,  
809 Coggon, M. M., Zhang, L., Feiner, P., Miller, D. O., Skog, K. M., Rivera-Rios, J. C., Dorris, M.,  
810 Olson, K. F., Koss, A., Wild, R. J., Brown, S. S., Goldstein, A. H., de Gouw, J. A., Brune,  
811 W. H., Keutsch, F. N., Seinfeld, J. H., and Wennberg, P. O.: Atmospheric fates of Criegee  
812 intermediates in the ozonolysis of isoprene, *Phys. Chem. Chem. Phys.*, 18, 10 241–10 254,  
813 <https://doi.org/10.1039/C6CP00053C>, <http://dx.doi.org/10.1039/C6CP00053C>, 2016.

814 O'Brien, R. E., Wang, B., Kelly, S. T., Lundt, N., You, Y., Bertram, A. K., Leone, S. R., Laskin,  
815 A., and Gilles, M. K.: Liquid–liquid phase separation in aerosol particles: Imaging at the  
816 nanometer scale, *Environ. Sci. Technol.*, 49, 4995–5002, [10.1021/acs.est.5b00062](https://doi.org/10.1021/acs.est.5b00062), 2015.

817 Pankow, J. F. and Asher, W. E.: SIMPOL.1: a simple group contribution method for predicting  
818 vapor pressures and enthalpies of vaporization of multifunctional organic compounds, *Atmos.  
819 Chem. Phys.*, 8, 2773–2796, <http://www.atmos-chem-phys.net/8/2773/2008/>, 2008.

820 Qiu, J., Liang, Z., Tonokura, K., Colussi, A. J., and Enami, S.: Stability of monoterpene-derived  
821 α-hydroxyalkyl-hydroperoxides in aqueous organic media – relevance to the fate of  
822 hydroperoxides in aerosol particle phases, *Environ. Sci. Technol.*, [10.1021/acs.est.9b07497](https://doi.org/10.1021/acs.est.9b07497),  
823 2020.



824 Rodríguez-Sevilla, J., Álvarez, M., Limiñana, G., Díaz, M. C.: Dilute SO<sub>2</sub> absorption equilibria  
825 in aqueous HCl and NaCl solutions at 298.15 K, *J. Chem. Eng. Data*, 47, 1339-1345, 2002.

826 Ruiz-Lopez, M.F., Francisco, J.S., Martins-Costa, M.T. and Anglada, J.M.: Molecular reactions  
827 at aqueous interfaces. *Nat. Rev. Chem.*, 1-17, 2020.

828 Seinfeld, J. H., and Pandis, S. N.: Atmospheric chemistry and physics: from air pollution to  
829 climate change, John Wiley & Sons, 2012.

830 Sha, T., Ma, X., Jia, H., Tian, R., Chang, Y., Cao, F., and Zhang, Y.: Aerosol chemical  
831 component: Simulations with WRF-Chem and comparison with observations in Nanjing, *Atmos.*  
832 *Environ.*, 218, 116982, <https://doi.org/10.1016/j.atmosenv.2019.116982>, 2019.

833 Shang, J., Li, J., Zhu, T.: Heterogeneous reaction of SO<sub>2</sub> on TiO<sub>2</sub> particles. *Sci. China Chem.*, 53,  
834 2637–2643, 2010.

835 Shi, Q., Davidovits, P., Jayne, J. T., Worsnop, D. R., and Kolb, C. E.: Uptake of gas-phase  
836 ammonia. 1. Uptake by aqueous surfaces as a function of pH, *J. Phys. Chem. A*, 103, 8812-8823,  
837 10.1021/jp991696p, 1999.

838 Song, M., Marcolli, C., Krieger, U. K., Zuend, A., and Peter, T.: Liquid–liquid phase separation  
839 in aerosol particles: dependence on O:C, organic functionalities, and compositional complexity,  
840 *Geophys. Res. Lett.*, 39, L19801, doi:10.1029/2012GL052807, 2012.

841 Song, S., Gao, M., Xu, W., Shao, J., Shi, G., Wang, S., Wang, Y., Sun, Y., and McElroy, M. B.:  
842 Fine-particle pH for Beijing winter haze as inferred from different thermodynamic equilibrium  
843 models, *Atmos. Chem. Phys.*, 18, 7423–7438, <https://doi.org/10.5194/acp-18-7423-2018>, 2018.

844 Song, S., Gao, M., Xu, W., Sun, Y., Worsnop, D. R., Jayne, J. T., Zhang, Y., Zhu, L., Li, M.,  
845 Zhou, Z., Cheng, C., Lv, Y., Wang, Y., Peng, W., Xu, X., Lin, N., Wang, Y., Wang, S., Munger,  
846 J. W., Jacob, D. J., and McElroy, M. B.: Possible heterogeneous chemistry of hydroxy  
847 methanesulfonate (HMS) in northern China winter haze, *Atmos. Chem. Phys.*, 19, 1357–1371,  
848 <https://doi.org/10.5194/acp-19-1357-2019>, 2019.

849 Su, H., Cheng, Y., and Poschl, U.: New multiphase chemical processes influencing atmospheric  
850 aerosols, air quality, and climate in the anthropocene, *Acc. Chem. Res.*, e1601530-2983,  
851 <https://doi.org/10.1021/acs.accounts.0c00246>, 2020.

852 Sun, Y., Wang, Z., Fu, P., Jiang, Q., Yang, T., Li, J., and Ge, X.: The impact of relative humidity  
853 on aerosol composition and evolution processes during wintertime in Beijing, China, *Atmos.*  
854 *Environ.*, 77, 927-934, 2013.

855 Surratt, J. D., Murphy, S. M., Kroll, J. H., Ng, N. L., Hildebrandt, L., Sorooshian, A.,  
856 Szmigielski, R., Vermeylen, R., Maenhaut, W., and Claeys, M.: Chemical composition of  
857 secondary organic aerosol formed from the photooxidation of isoprene, *J. Phys. Chem. A*, 110,  
858 9665-9690, 2006.

859 Thornton, J. A., Braban, C. F., and Abbatt, J. P. D.: N<sub>2</sub>O<sub>5</sub> hydrolysis on sub-micron organic  
860 aerosols: the effect of relative humidity, particle phase, and particle size, *Phys. Chem. Chem*  
861 *Phys.*, 5, 4593–4603, <https://doi.org/10.1039/B307498F>, 2003.

862 Tie, X., Brasseur, G., Emmons, L., Horowitz, I., and Kinnison, D.: Effects of aerosols on  
863 tropospheric oxidants: a global model study, *J. Geophys. Res. Atmos.*, 106, 22931–22964, 2001.

864 Tong, H., Arangio, A. M., Lakey, P. S. J., Berkemeier, T., Liu, F., Kampf, C. J., Brune, W. H.,  
865 Pöschl, U., and Shiraiwa, M.: Hydroxyl radicals from secondary organic aerosol decomposition  
866 in water, *Atmos. Chem. Phys.*, 16, 1761–1771, doi:10.5194/acp-16-1761-2016, 2016.

867 Usher, C. R., Al-Hosney, H., Carlos-Cuellar, S., and Grassian, V. H.: A laboratory study of the  
868 heterogeneous uptake and oxidation of sulfur dioxide on mineral dust particles, *J. Geophys. Res.*,  
869 107, 4713, doi:10.1029/2002JD002051, 2002.

870 Varutbangkul, V., Brechtel, F. J., Bahreini, R., Ng, N. L., Keywood, M. D., Kroll, J. H., Flagan,  
871 R. C., Seinfeld, J. H., Lee, A., and Goldstein, A. H.: Hygroscopicity of secondary organic  
872 aerosols formed by oxidation of cycloalkenes, monoterpenes, sesquiterpenes, and related  
873 compounds, *Atmos. Chem. Phys.*, 6, 2367–2388, [http://www.atmos-chem-phys.net/6/23](http://www.atmos-chem-phys.net/6/2367/2006/)  
874 [67/2006/](http://www.atmos-chem-phys.net/6/2367/2006/), 2006.

875 Veghte, D. P., Altaf, M. B., and Freedman, M. A.: Size dependence of the structure of organic  
876 aerosol, *J. Am. Chem. Soc.*, 135, 16046–16049, 2013.

877 Wang, G., Zhang, R., Gomez, M. E., Yang, L., Zamora, M. L., Hu, M., Lin, Y., Peng, J., Guo, S.,  
878 and Meng, J.: Persistent sulfate formation from London Fog to Chinese haze, *Proc. Natl. Acad.*  
879 *Sci. U. S. A.*, 113, 13630-13635, 2016.

880 Wang, S., Ye, J., Soong, R., Wu, B., Yu, L., Simpson, A. J., and Chan, A. W. H.: Relationship  
881 between chemical composition and oxidative potential of secondary organic aerosol from  
882 polycyclic aromatic hydrocarbons, *Atmos. Chem. Phys.*, 18, 3987-4003, 2018.

883 Wang, S., Zhou, S., Tao, Y., Tsui, W. G., Ye, J., Yu, J. Z., Murphy, J. G., McNeill, V. F.,  
884 Abbatt, J. P. D., and Chan, A. W. H.: Organic peroxides and sulfur dioxide in aerosol: Source of  
885 particulate sulfate, *Environ. Sci. Technol.*, 53, 10695-10704, 10.1021/acs.est.9b02591, 2019.

886 Wang, X.; Gemayel, R.; Hayeck, N.; Perrier, S.; Charbonnel, N.; Xu, C.; Chen, H.; Zhu, C.;  
887 Zhang, L.; Wang, L.; Nizkorodov, S. A.; Wang, X.; Wang, Z.; Wang, T.; Mellouki, A.; Riva, M.;  
888 Chen, J.; George, C. Atmospheric photosensitization: A new pathway for sulfate formation,  
889 *Environ. Sci. Technol.*, 54, 3114-3120, 2020.

890 Wang, Y., Zhang, Q., Jiang, J., Zhou, W., Wang, B., He, K., Duan, F., Zhang, Q., Philip, S., and  
891 Xie, Y.: Enhanced sulfate formation during China's severe winter haze episode in January 2013  
892 missing from current models, *J. Geophys. Res. Atmos.*, 119, 10425–10440,  
893 <https://doi.org/10.1002/2013JD021426>, 2014.

894 Wei, H., Vejerano, E. P., Leng, W., Huang, Q., Willner, M. R., Marr, L. C., and Vikesland, P. J.:  
895 Aerosol microdroplets exhibit a stable pH gradient, *Proc. Natl. Acad. Sci. U. S. A.*, 115, 7272,  
896 10.1073/pnas.1720488115, 2018.

897 Xu, L., Guo, H., Boyd, C. M., Klein, M., Bougiatioti, A., Cerully, K. M., Hite, J. R., Isaacman-  
898 VanWertz, G., Kreisberg, N. M., and Knote, C.: Effects of anthropogenic emissions on aerosol  
899 formation from isoprene and monoterpenes in the southeastern United States, *Proc. Natl. Acad.*  
900 *Sci. U. S. A.*, 112, 37-42, 2015.

901 Yang, Y., Wang, H., Smith, S. J., Easter, R., Ma, P.-L., Qian, Y., Yu, H., Li, C., and Rasch, P. J.:  
902 Global source attribution of sulfate concentration and direct and indirect radiative forcing,  
903 *Atmos. Chem. Phys.*, 17, 8903–8922, <https://doi.org/10.5194/acp17-8903-2017>, 2017.

904 Yao, M., Zhao, Y., Hu, M., Huang, D., Wang, Y.C., Yu, J. Z., and Yan, N.: Multiphase reactions  
905 between secondary organic aerosol and sulfur dioxide: kinetics and contributions to sulfate  
906 formation and aerosol aging, *Environ. Sci. Tech. Let.* 6, 768-774, 10.1021/acs.estlett.9b00657,  
907 2019.

908 Ye, J., Gordon, C. A., and Chan, A. W. H: Enhancement in secondary organic aerosol formation  
909 in the presence of preexisting organic particle, *Environ. Sci. Technol.*, 50, 3572-3579, 2016.

910 Ye, J., Abbatt, J. P. D., and Chan, A. W. H.: Novel pathway of SO<sub>2</sub> oxidation in the atmosphere:  
911 reactions with monoterpene ozonolysis intermediates and secondary organic aerosol, *Atmos.*  
912 *Chem. Phys.*, 18, 5549–5565, <https://doi.org/10.5194/acp18-5549-2018>, 2018.

913 Yee, L. D., Isaacman-VanWertz, G., Wernis, R. A., Kreisberg, N. M., Glasius, M., Riva, M.,  
914 Surratt, J. D., de Sá, S. S., Martin, S. T., Alexander, M. L., Palm, B. B., Hu, W., Campuzano-  
915 Jost, P., Day, D. A., Jimenez, J. L., Liu, Y., Misztal, P. K., Artaxo, P., Viegas, J., Manzi, A., de  
916 Souza, R. A. F., Edgerton, E. S., Baumann, K., and Goldstein, A. H.: Natural and  
917 anthropogenically influenced isoprene oxidation in southeastern United States and central  
918 Amazon, *Environ. Sci. Technol.*, 54, 5980-5991, 10.1021/acs.est.0c00805, 2020.

919 You, Y., Renbaum-Wolff, L., Bertram, A. K: Liquid-liquid phase separation in particles  
920 containing organics mixed with ammonium sulfate, ammonium bisulfate, ammonium nitrate or  
921 sodium chloride, *Atmos. Chem. Phys.*, 13, 11723–11734, [https://doi.org/10.5194/acp-13-11723-](https://doi.org/10.5194/acp-13-11723-2013)  
922 2013, 2013.

923 You, Y., Smith, M. L., Song, M., Martin, S. T., and Bertram, A. K.: Liquid–liquid phase  
924 separation in atmospherically relevant particles consisting of organic species and inorganic salts,  
925 *Int. Rev. Phys. Chem.*, 33, 43–77, doi:10.1080/0144235X.2014.890786, 2014.

926 Zhang, S., Xing, J., Sarwar, G., Ge, Y., He, H., Duan, F., Zhao, Y., He, K., Zhu, L. and Chu, B.:  
927 Parameterization of heterogeneous reaction of SO<sub>2</sub> to sulfate on dust with coexistence of NH<sub>3</sub>  
928 and NO<sub>2</sub> under different humidity conditions, *Atmos. Environ.*, 208, 133-140, 2019.

929 Zhao, Y., Liu, Y., Ma, J., Ma, Q., and He, H.: Heterogeneous reaction of SO<sub>2</sub> with soot: The  
930 roles of relative humidity and surface composition of soot in surface sulfate formation, *Atmos.*  
931 *Environ.*, 152, 465-476, 2017.

932 Zheng, B., Zhang, Q., Zhang, Y., He, K. B., Wang, K., Zheng, G. J., Duan, F. K., Ma, Y. L., and  
933 Kimoto, T.: Heterogeneous chemistry: a mechanism missing in current models to explain  
934 secondary inorganic aerosol formation during the January 2013 haze episode in North China,  
935 *Atmos. Chem. Phys.*, 15, 2031–2049, doi:10.5194/acp-15-2031-2015, 2015.

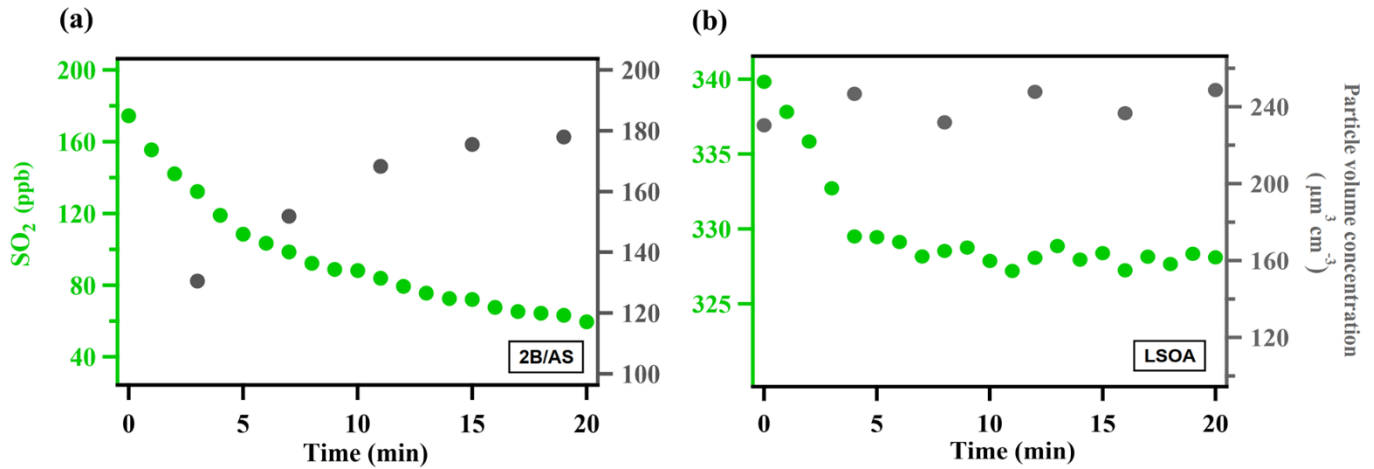
936 Zheng, G. J., Duan, F. K., Su, H., Ma, Y. L., Cheng, Y., Zheng, B., Zhang, Q., Huang, T.,  
937 Kimoto, T., Chang, D., Pöschl, U., Cheng, Y. F., and He, K. B.: Exploring the severe winter haze  
938 in Beijing: the impact of synoptic weather, regional transport and heterogeneous reactions,  
939 *Atmos. Chem. Phys.*, 15, 2969–2983, doi:10.5194/acp-15-2969-2015, 2015.

940

941

942

943



944

945 **Figure 1.** Typical evolution of the species monitored during  $\gamma_{\text{SO}_2}$  measurement for (a)  
 946 ammonium sulfate mixed with 2-butanone organic peroxide (2B/AS, Expt. 16) and (b) limonene  
 947 SOA (LSOA, Expt. 27). Particle volume concentrations measured by SMPS have been corrected  
 948 for wall loss assuming a pseudo first-order loss rate (Ye et al., 2016).  $\gamma_{\text{SO}_2}$  was calculated for the  
 949 initial portion of the decay (first 7 minutes).

950

951

952

953

954

955

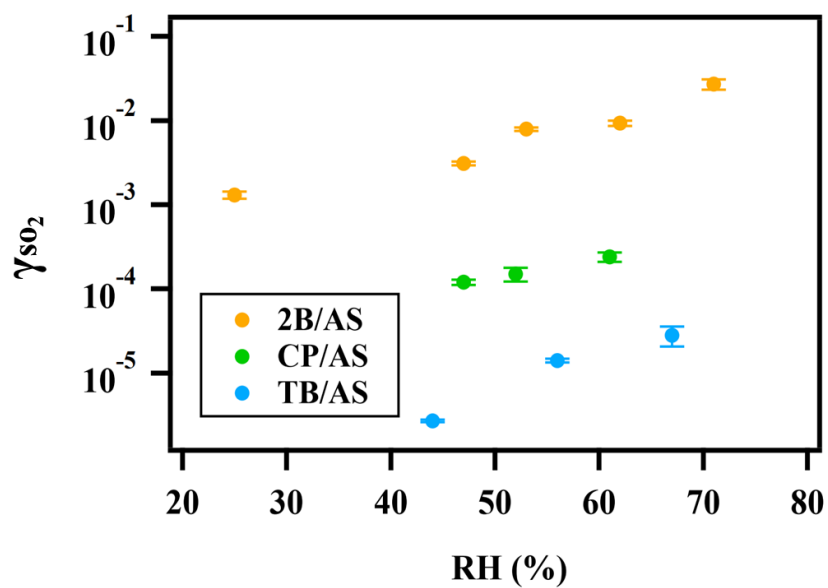
956

957

958

959

960



961  
962 **Figure 2.** Exponential relationship between  $\gamma_{\text{SO}_2}$  and RH for ammonium sulfate aerosol  
963 containing 2-butanone peroxide (2B), cumene hydroperoxide (CP), tert-butyl hydroperoxide  
964 (TB).

965

966

967

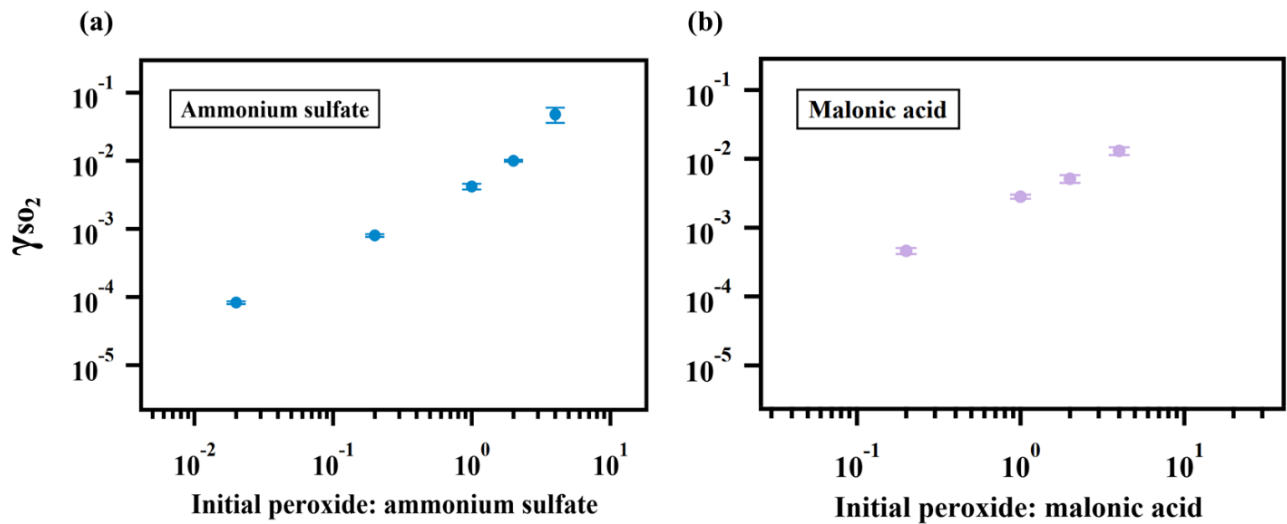
968

969

970

971

972



973

974 **Figure 3.** Relationship between  $\gamma_{SO_2}$  and particulate peroxide content.  $\gamma_{SO_2}$  for ammonium sulfate  
 975 (a) and malonic acid aerosol (b) containing different amount of 2-butanone peroxide are shown  
 976 here. The observed dependence of  $\gamma_{SO_2}$  on the amount of peroxide injected are linear since the  
 977 slopes of the relationship are both nearly 1 in (a) and (b).

978

979

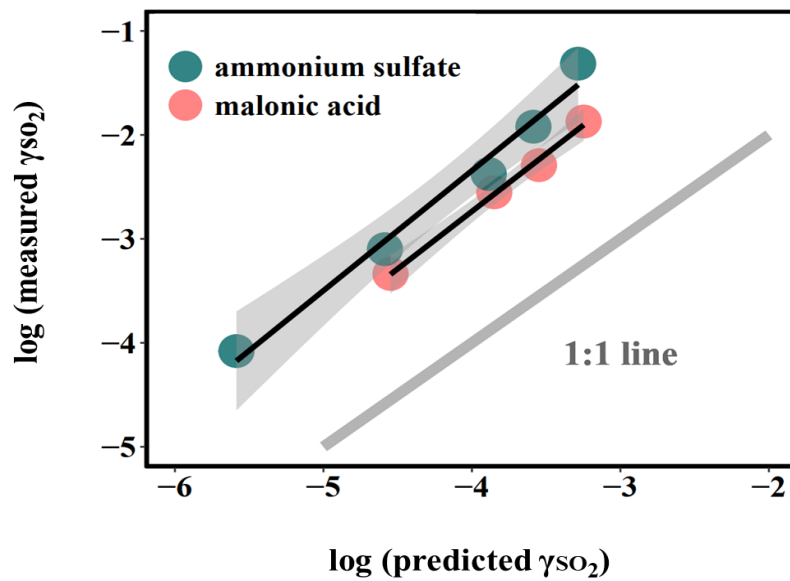
980

981

982

983

984



985

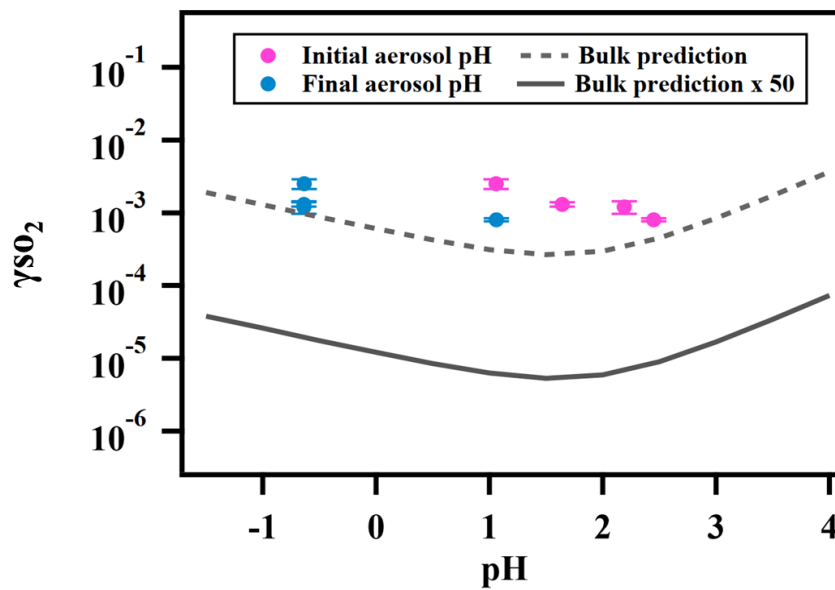
986 **Figure 4.** Relationship between measured  $\gamma_{SO_2}$  and  $\gamma_{SO_2}$  predicted by Eqn. 4. The large deviation  
 987 from the 1:1 line, which represents the difference between the measured uptake coefficient and  
 988 predicted values based on kinetics in the dilute aqueous phase, indicates that aerosol reactive  
 989 uptake is significantly faster than reactions in dilute aqueous phase. This enhancement is likely  
 990 driven in part by high ionic strengths, as the difference between measured  $\gamma_{SO_2}$  and predicted  $\gamma_{SO_2}$   
 991 are consistently higher for organic peroxide containing ammonium sulfate (high ionic strength)  
 992 than for that mixed with malonic acid (lower ionic strength).

993

994

995

996



997

998 **Figure 5.** Relationship between  $\gamma_{SO_2}$  and aerosol phase pH for ammonium sulfate aerosol  
 999 containing 2-butanone peroxide.

1000

1001

1002

1003

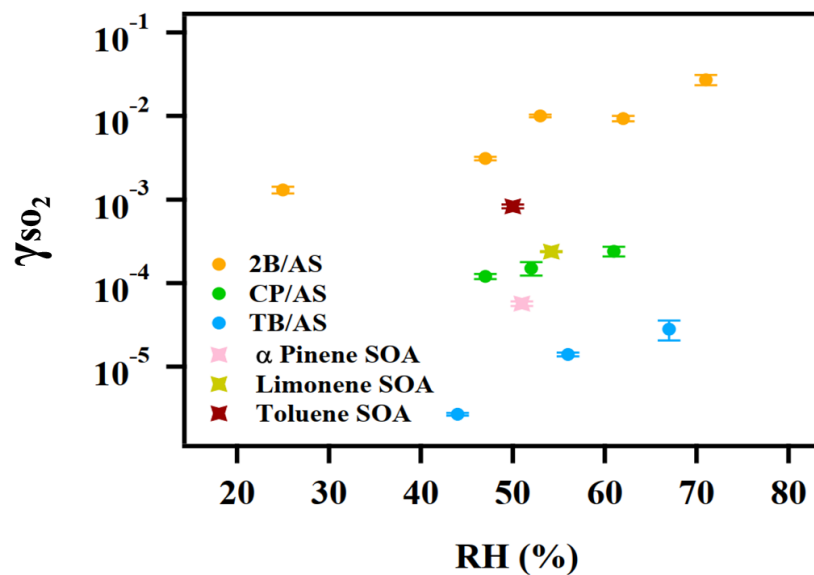
1004

1005

1006

1007





1008

1009 **Figure 6.**  $\gamma_{SO_2}$  measured for different types of organic aerosol. The reactive uptake coefficient of  
 1010  $SO_2$  onto SOA are on the order of  $10^{-4}$ .

1011

1012

1013

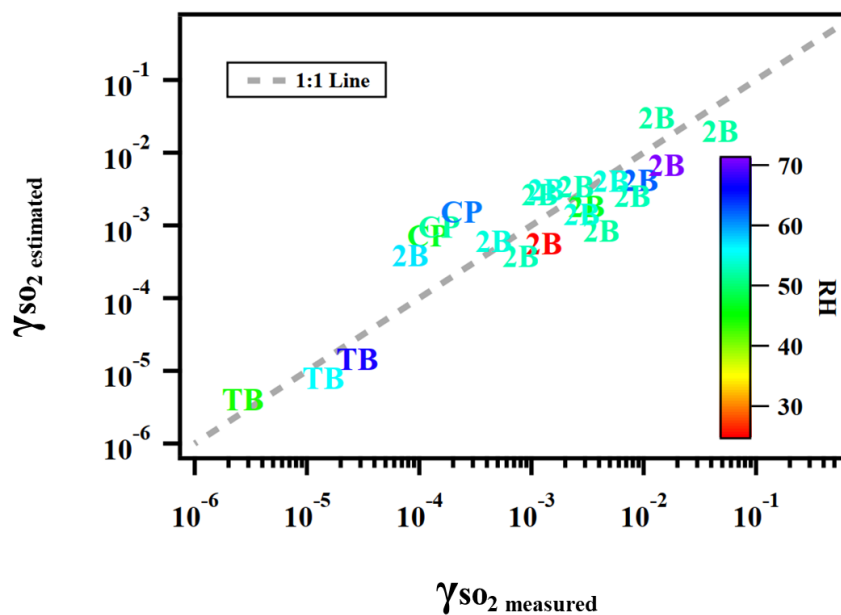
1014

1015

1016

1017

1018



1019

1020 **Figure 7.** Predicted  $\gamma_{SO_2}$  using Equation (8) versus measured  $\gamma_{SO_2}$  for ammonium sulfate or  
 1021 malonic acid aerosol containing 2-butanone peroxide (2B), cumene hydroperoxide (CP), tert-  
 1022 butyl hydroperoxide (TB) under different experimental conditions.

1023

1024

1025

1026

1027

1028

1029